

**Physically asymmetric division of the *C. elegans* zygote ensures
invariably successful embryogenesis**

Radek Jankele ¹, Rob Jelier ², Pierre Gönczy ¹

¹ Swiss Institute for Experimental Cancer Research (ISREC), School of Life Sciences, Swiss
Federal Institute of Technology Lausanne (EPFL), Switzerland

² Centre of Microbial and Plant Genetics, Katholieke Universiteit Leuven, Belgium

Correspondence: pierre.gonczy@epfl.ch

Keywords: *C. elegans*, zygote, asymmetric cell division, *lin-5*, cell lineaging, division timing,
cell positioning, division orientation

Abstract

Asymmetric divisions that yield daughter cells of different sizes are frequent during early embryogenesis, but the importance of such a physical difference for successful development remains poorly understood. Here, we investigated this question using the first division of *C. elegans* embryos, which yields a large AB cell and a small P₁ cell. We equalized AB and P₁ sizes using acute genetic inactivation or optogenetic manipulation of the spindle positioning protein LIN-5. We uncovered that only some embryos tolerated equalization, and that there was a size asymmetry threshold for viability. Cell lineage analysis of equalized embryos revealed an array of defects, including faster cell cycle progression in P₁ descendants, as well as defects in cell positioning, division orientation and cell fate. Moreover, equalized embryos were more susceptible to external compression. Overall, we conclude that unequal first cleavage is essential for invariably successful embryonic development of *C. elegans*.

Introduction

Asymmetric divisions generate cell fate diversity during development and differentiation. Daughter cells of such divisions can differ not only in their asymmetric inheritance of fate determinants, but also in their relative size. Such physically unequal asymmetric divisions are widespread during development. For instance, in *C. elegans* larvae, QR.a neuroblasts divide unequally owing to the asymmetric distribution of the non-muscle myosin II NMY-2, resulting in a larger daughter with a neuronal fate and a smaller daughter that undergoes apoptosis (Ou et al., 2010). Equalizing QR.a division through NMY-2 manipulation results in two cells adopting the neuronal fate (Ou et al., 2010). Likewise, *Drosophila* stem-like larval neuroblasts divide unequally to regenerate a larger neuroblast and a smaller ganglion mother cell that differentiates towards a neuronal fate. Experimentally induced size equalization of the neuroblast division prevents such differentiation, despite proper asymmetric inheritance of the neuronal fate determinant Prospero (Cabernard and Doe, 2009; Kitajima et al., 2010). These examples illustrate how size differences can have a drastic consequence on the fate of resulting daughter cells. Physically unequal divisions are particularly prevalent during early embryogenesis in many systems, but the specific importance of size differences in the cases for successful completion of development has been scarcely addressed.

Early embryogenesis in the nematode *C. elegans* entails several asymmetric divisions, including ones that yield daughter cells of different sizes (reviewed in Rose and Gönczy, 2014). The first of these is the unequal cleavage of the one-cell stage embryo (hereafter zygote) into the larger anterior cell AB and the smaller posterior cell P₁, corresponding respectively to ~60% and ~40% of total embryo size. The variability in this size difference is minimal in the wild type (Kemphues et al., 1988), suggestive of functional importance. Further support for such importance comes from the fact that unequal first cleavage occurs throughout the entire *Rhabditida* order, which is estimated to encompass an evolutionary distance as large as that between echinoderms and mammals (Kiontke and Fitch, 2005), although the

55 extent of size asymmetry varies between nematode species within this order (Brauchle et al.,
56 2009; Valfort et al., 2018).

57 The unequal cleavage of the *C. elegans* zygote results from a rapid sequence of
58 events that begins after fertilization (reviewed in Rose and Gönczy, 2014). First, symmetry of
59 the zygote is broken by the centrosomes derived from the sperm (Goldstein and Hird, 1996;
60 Sadler and Shakes, 2000). Thereafter, the contractile cortical acto-myosin network moves
61 towards the future embryo anterior (Munro et al., 2004), accompanied by the establishment of
62 mutually exclusive cortical domains of PAR polarity domains, with aPKC-3/PAR-3/PAR-6 at
63 the anterior and PAR-1/PAR-2/LGL-1 at the posterior (reviewed in Kemphues and Strome,
64 1997; Rose and Gönczy, 2014). The PAR polarity network then ensures the asymmetric
65 distribution of proteins and mRNAs through the action of polarity mediators, including the
66 RNA-binding proteins MEX-5/6, which are present in an anterior-posterior (A-P) gradient prior
67 to first cleavage (Schubert et al., 2000).

68 A-P polarity cues also direct asymmetric positioning of the mitotic spindle, which is
69 located slightly off-center towards the posterior side by the end of anaphase, thus dictating
70 unequal first cleavage (Grill et al., 2001). Asymmetric spindle positioning relies on an
71 evolutionarily conserved ternary complex that anchors the molecular motor dynein at the cell
72 cortex (reviewed in Kotak and Gönczy, 2013). In *C. elegans*, this ternary complex comprises
73 the membrane associated Gα proteins GOA-1 and GPA-16, the TPR and GoLoCo domain-
74 containing proteins GPR-1/2, as well as the coiled-coil protein LIN-5, which interacts with a
75 dynein-dynactin motor complex (Colombo et al., 2003; Gotta et al., 2003; Gotta and Ahringer,
76 2001; Srinivasan et al., 2003). Dynein thus anchored at the cell cortex is thought to exert a
77 pulling force on the plus-end of depolymerizing astral microtubules and, thereby, on the
78 connected spindle poles. In response to A-P polarity cues, more GPR-1/2 and possibly LIN-5
79 are present on the posterior cortex, resulting in a larger net force pulling on the posterior
80 spindle pole, leading to the unequal cleavage of the zygote into the larger AB cell and the
81 smaller P₁ cell (Colombo et al., 2003; Gotta et al., 2003; Grill et al., 2003, 2001; Park and
82 Rose, 2008; Tsou et al., 2003).

During subsequent stages of *C. elegans* embryogenesis, most cells derived from AB divide symmetrically and with nearly synchronous timing, whereas P₁ descendants undergo three additional asymmetric divisions, generating sister lineages with asynchronous division timing (Sulston et al., 1983). Overall, this leads to the generation of seven founder cells that will each yield specific tissues; for instance, E will give rise to the intestine and P₄ to the germline (Sulston et al., 1983). The fate of each founder cell is specified by asymmetrically distributed maternally provided components, together with regulated protein translation and degradation mechanisms operating in the embryo (reviewed in Rose and Gönczy, 2014; Zacharias and Murray, 2016). Global activation of zygotic transcription occurs at the ~26-cell stage (Powell-Coffman et al., 1996; Schauer and Wood, 1990), which is also when the onset of gastrulation is apparent by ingression of the E descendants Ea/Ep from the embryo periphery (reviewed in Goldstein and Nance, 2020). Whereas Ea/Ep descendants adopt an intestinal fate in a cell-autonomous manner, for other cells proper fate acquisition and behavior, including division orientation, relies on interactions among neighbors (reviewed in Goldstein and Nance, 2020; Mango, 2009; Rose and Gönczy, 2014). Overall, as a result of stereotyped division timing, cell positioning, division orientation and fate allocation, the hermaphrodite *C. elegans* embryo invariably hatches with 558 cells (Sulston et al., 1983).

Despite the wealth of knowledge brought by decades of investigating developmental mechanisms in *C. elegans*, the specific importance of the size difference component of asymmetric division in the early embryo is not clear, including for the unequal division of the zygote. Investigating this question requires to specifically alter the size of the daughter cells resulting from first cleavage without altering A-P polarity or compromising subsequent cell divisions. This has been challenging: although *par* mutant embryos undergo equal first divisions. This has been challenging: although *par* mutant embryos undergo equal first cleavage, A-P polarity is abolished entirely in these cases (Kemphues et al., 1988). Moreover, whereas depletion of *goa-1/gpa-16*, *gpr-1/2* or *lin-5* by RNAi results in equal first division without A-P polarity defects, such embryos exhibit severe cell division defects in subsequent cycles (Colombo et al., 2003; Fisk Green et al., 2004; Gotta et al., 2003; Gotta and Ahringer, 2001; Lorson et al., 2000; Srinivasan et al., 2003). Here, we specifically equalized AB and P₁

without altering A-P polarity or disrupting later cell divisions using acute genetic inactivation or optogenetic manipulation of LIN-5, allowing us to address specifically the importance of the physical asymmetry of the *C. elegans* zygote division.

Results

Altering cell size asymmetry through manipulation of *lin-5* function

To address whether the size difference between AB and P₁ that derives from the unequal division of the *C. elegans* zygote is important for subsequent development, we took advantage of the temperature-sensitive *lin-5(ev571)* mutant allele (Lorson et al., 2000). We discovered that shifting *lin-5(ev571)* zygotes from 17°C to 27°C for ~5 min during mitosis results in the spindle remaining in the cell center, yielding AB and P₁ cells of more similar sizes than normal (Fig. 1A-C, Figure 1 - supplement 1, Video 1-3). Such embryos are referred to as “upshifted *lin-5(ev571)*” hereafter. There was a slight variability in the size of AB relative to that of the entire zygote in these embryos (51.2 % ± 2.8 standard deviation (SD), N=257). Moreover, we found that inactivation of function was readily reversible, since returning upshifted *lin-5(ev571)* embryos to 17°C after the ~5 min upshift rapidly restored LIN-5 function, allowing subsequent cell divisions to proceed (see below). Furthermore, to control for potential effects of the *lin-5(ev571)* mutation unrelated to AB and P₁ equalization, early 2-cell stage *lin-5(ev571)* embryos were shifted from 17°C to 27°C for ~5 min; such embryos are referred to as “controls” throughout the manuscript.

Severe or complete depletion of *lin-5* function does not impair A-P polarity (Srinivasan et al., 2003), and we found the same to be true upon acute LIN-5 inactivation in upshifted *lin-5(ev571)* embryos, as evidenced by the normal distribution of the posterior polarity protein PAR-2 (Fig. 1 supplement 2A, 2B). Moreover, the polarity mediator MEX-5, which is enriched in the anterior cytoplasm of the wild-type zygote in response to A-P polarity cues (Cuenca et al., 2003; Schubert et al., 2000), was localized similarly in control and upshifted *lin-5(ev571)* embryos, resulting in MEX-5 enrichment in AB following first division (Fig. 1 supplement 2C).

In addition, as anticipated from the more centrally located first cleavage furrow, slightly more MEX-5 was present in P_1 in upshifted *lin-5(ev571)* embryos than in the control (Fig. 1 supplement 2D). Taken together, these observations indicate that upshifted *lin-5(ev571)* zygotes exhibit normal A-P polarity, providing us with an experimental means to address specifically the impact of cell size asymmetry.

In search for a complementary method to equalize first division, we reasoned that optogenetic recruitment of LIN-5 to the anterior cortex could counteract the larger posterior forces normally acting on astral microtubules, thus maintaining the spindle in the center (Fielmich et al., 2018). We used an extant worm strain expressing both LOV::PH::GFP bound to the plasma membrane and endogenously tagged LIN-5::ePDZ::mCherry, which can thus be recruited to the desired portion of the plasma membrane by transient local induction of LOV<-> ePDZ interaction using 488 nm laser light (Fielmich et al., 2018) (Fig. 1D, 1E). As anticipated, we found that acute recruitment of LIN-5::ePDZ::mCherry to a small region of the anterior cortex can maintain the spindle in the center of the zygote, producing similarly sized AB and P_1 cells (Fig. 1F, Video 4).

Overall, we conclude that two means of balancing anterior and posterior pulling forces during mitosis can serve to equalize the first division.

First cleavage equalization can be tolerated up to a size asymmetry threshold

To assess the potential importance of the size difference between AB and P_1 for subsequent development, we utilized time-lapse microscopy to analyze upshifted *lin-5(ev571)* embryos and optogenetically manipulated embryos following return to their respective permissive conditions, scoring embryonic lethality at the motile 3-fold stage or at hatching (Materials and Methods). We found that those upshifted *lin-5(ev571)* embryos that died invariably failed to elongate into a worm-shape towards the end of embryogenesis, reflecting a failure in ventral closure of the epidermis that was accompanied by extrusion of endodermal and mesodermal tissues as muscle contraction began (Fig. 1C, Fig. 1 – supplement 3, Video 5 and Video 6; n=92). The terminal embryonic phenotype of optogenetically manipulated embryos that died

was likewise characterized by a failure in ventral epidermal closure, with the exception of one embryo that died as an unhatched larva (n=26). Moreover, we found several post-embryonic phenotypes amongst upshifted *lin-5(ev571)* animals that hatched, including death during larval stages and reduced adult fertility (Fig. 1 – supplement 3C), demonstrating that equalizing the first division can result in lethality beyond embryogenesis.

We took advantage of the slight variability in relative AB size following equalization to ask whether this trait correlated with the incidence of embryonic lethality. As shown in Figure 2A and 2B, we observed that whereas control embryos exhibited nearly identical lethality compared to *lin-5(ev571)* embryos maintained at 17°C (~7%), lethality of upshifted *lin-5(ev571)* embryos gradually increased as AB and P₁ became closer in size, from ~24% when relative AB size was (56-54]%, to ~75% when it was (50-48]% (refer to Supplementary File 6 for statistical analyses throughout the manuscript). We found a similar gradual increase of embryonic lethality when AB and P₁ became closer in size in optogenetically manipulated embryos (Fig. 2C, 2D), which however exhibited ~23% lethality even when not exposed to 488 nm laser light. In addition, we found in both experimental settings that embryos with a relative AB size smaller than 48% invariably died (Fig. 2B, 2D; “inverted embryos” hereafter).

Taken together, these findings establish that first cleavage equalization can be tolerated to some extent, since a subset of embryos with similar AB and P₁ sizes survive. However, other such embryos die, suggesting that the unequal first cleavage is required for invariably successful embryogenesis. Furthermore, our findings reveal a size asymmetry threshold at the 2-cell stage below which embryogenesis always fails.

Decreased asynchrony between AB and P₁ upon first division equalization does not cause lethality of equalized embryos

We investigated further the consequences of rendering AB and P₁ similar in size. We utilized the *lin-5(ev571)* upshift setting for all experiments described hereafter, because the optogenetic strain exhibited higher background lethality and was not amenable to investigation

with fluorescently labeled markers since both GFP and mCherry channels are already occupied.

We first report our analysis of cell division timing. In the wild type, AB divides before P₁, in part owing to a size difference between the two cells (Brauchle et al., 2003). We addressed whether such a reduction in asynchrony was recapitulated in upshifted *lin-5(ev571)* embryos, using H2B::mCherry to precisely time anaphase onset. As shown in Figure 2E, we indeed found a strong correlation between relative AB size and extent of division asynchrony, confirming that the size difference between AB and P₁ contributes to their division asynchrony. Moreover, inverted embryos retained residual asynchrony (Fig. 2E), verifying that cell size is only one of the factors dictating such asynchrony (Budirahardja and Gönczy, 2008; Rivers et al., 2008).

Could the reduction in division asynchrony between AB and P₁ cause the lethality of upshifted *lin-5(ev571)* embryos? We reasoned that if this were the case, then survival should be higher in upshifted *lin-5(ev571)* embryos in which asynchrony between the two cells was experimentally restored to the wild-type timing. Therefore, we set out to specifically slow down the cell cycle of P₁ in upshifted *lin-5(ev571)* embryos by directing a 405 nm laser onto its nucleus, adapting a method used previously for endodermal cells in the worm (Lee et al., 2006). We determined a non-lethal irradiation regime that retarded P₁ division timing in the wild type by 132 ± 94 s on average (n=7), but did not cause lethality (Materials and Methods). We found that a similar treatment in upshifted *lin-5(ev571)* embryos restored the extent of asynchrony between AB and P₁ to that of control embryos (Fig. 2F). Despite this, however, viability was not rescued (Fig. 2F), leading us to conclude that reduction in division asynchrony between AB and P₁ *per se* is not responsible for the lethality of upshifted *lin-5(ev571)* embryos.

Interestingly, in addition, we found a severe phenotype arising at the 4-cell stage in a minor fraction of upshifted *lin-5(ev571)* embryos, which we reasoned might be related to reduced division asynchrony between AB and P₁. In the wild type, division asynchrony results in the AB spindle elongating before the P₁ spindle, and thereby to an oblique positioning of the

AB daughter cells due to the geometrical constraints imposed by the eggshell (Fig. 2 supplement 1A). This leads to a characteristic rhomboid arrangement at the 4-cell stage, with the P_1 daughter P_2 contacting the AB daughter ABp (Fig. 2 supplement 1A). P_2 expresses the Delta-like ligand APX-1, which interacts with the Notch receptor GLP-1 present on ABp, thereby instructing ABp descendants to adopt neural and epidermal fates (Mango et al., 1994b; Mello et al., 1994; Shelton and Bowerman, 1996) (Fig. 2 supplement 1B). We found that ~4% of upshifted *lin-5(ev571)* embryos adopted an abnormal T-like arrangement at the 4-cell stage (T-arrangement thereafter) (Fig. 2 supplement 1C; Video 7; n=257). In such embryos, P_2 cannot contact ABp and, by inference, Delta/Notch signaling cannot take place between the two cells (Fig. 2 supplement 1D). As anticipated from such lack of signaling, all embryos with a T-arrangement at the 4-cell stage later died (n=11).

Overall, we conclude that reduced division asynchrony between AB and P_1 *per se* is not responsible for the lethality of most upshifted *lin-5(ev571)* embryos. Moreover, we find that a minor fraction of upshifted *lin-5(ev571)* embryos lack contact between P_2 and ABp and, thereby, a critical Delta/Notch induction event, illustrating how the size difference between AB and P_1 can contribute to successful fate acquisition.

Comprehensive 4D cell lineaging to monitor development of equalized embryos

To reach a more comprehensive understanding of potential deviations from normal development following first division equalization, we conducted systematic 4D lineage tracing using nuclear H2B::mCherry as a proxy for cell position (Bao et al., 2006; Jelier et al., 2016; Krüger et al., 2015). We collected data up to the ~120-cell stage, assessing 13 features for each cell, including division timing, cell position and division orientation, resulting in up to ~2000 data points per embryo, although not all stages or features could be scored in every instance (see Supplementary File 1 for information regarding each lineaged embryo and Supplementary File 2 for individual cell data). The entire lineaging data set is available at <https://github.com/UPGON/worm-rules-eLife>.

The lineaging data set comprised wild-type embryos (wild-type, n=10), *lin-5(ev571)* embryos shifted early in the 2-cell stage (control, n=18), as well as upshifted *lin-5(ev571)* embryos that were equalized (empirically defined as having a relative AB size of 48-53%), and that either lived (equalized alive, n=21) or died (equalized dead, n=28). There was no significant difference in relative AB size between these two equalized groups (50.6% in both; p=0.99), so that their distinct fate later in embryogenesis cannot be attributed to a size difference at the 2-cell stage. In addition, we lineaged *lin-5(ev571)* embryos with a <48% relative AB size, all of which died (inverted, n=7). Given their severe and early departure from normality, we did not lineage the minor fraction of *lin-5(ev571)* embryos with a 4-cell stage T-arrangement.

We set out to mine this rich data set to uncover deviations from normal development following AB and P₁ equalization, comparing wild-type and control embryos with equalized *lin-5(ev571)* and inverted *lin-5(ev571)* embryos. In addition, we investigated whether differences could be unveiled between equalized alive and equalized dead *lin-5(ev571)* embryos to identify features that may cause lethality in the latter group.

Lineaging reveals global alteration in cell cycle progression in the P₁ lineage and an altered sequence of cell division in equalized embryos

We first report our analysis of temporal aspects in the lineaging data. Plotting separately the proliferation of cells descending from AB and P₁ (hereafter referred to as AB and P₁ lineage), we observed no statistically significant difference in division timing in the AB lineage between wild-type or control and equalized or inverted *lin-5(ev571)* embryos (Fig. 3A – overlapping confidence intervals, Supplementary File 2). In stark contrast, we found a clear difference in the P₁ lineage, where cell number increased more rapidly in equalized and in inverted embryos compared to wild-type or control embryos (Fig. 3B). Furthermore, cell cycle duration in equalized *lin-5(ev571)* embryos was rarely correlated with relative AB size for AB descendants, but highly correlated for most P₁ descendants (Fig. 3. supplement 1, Supplementary File 3).

Investigating cell cycle duration in individual blastomeres revealed that the germ line precursor P_4 was most affected, with the cell cycle being ~33% shorter in equalized embryos compared to the control (Fig. 3C, $p < 0.001$ with Welch's two-sample t test, which is used also hereafter unless stated otherwise). Interestingly, we also uncovered a deviation from the normal division pattern in the P_4 lineage suggestive of fate transformation. Whereas P_4 normally undergoes a single division (Fig. 4D, top and Fig. 4E), we found that it underwent at least one additional division in ~35% of equalized *lin-5(ev571)* embryos ($n=36$), and in all four inverted *lin-5(ev571)* embryos scored for this trait (Fig. 4D, bottom and Fig. 4E). Overall, we conclude that following first division equalization, the cell cycle is shortened most in the germ line precursor P_4 , the fate of which is also imparted less faithfully.

We found in addition that faster cycling in the P_1 lineage of equalized embryos eventually changed the relative order of cell division during development (Fig. 3F). Notably, the division of the P_1 descendants Ea/Ep, D, Da and P_4 occurred before that of the corresponding AB lineage cells (Fig. 3F, red arrows). Could such an altered sequence of events in the AB versus the P_1 lineage contribute to the lethality of equalized *lin-5(ev571)* embryos? To address this question, we investigated whether there was a statistically significant difference in cell cycle duration or division timing comparing individual cells in equalized alive and equalized dead embryos, but found none (Supplementary File 2, Welch's t tests with Benjamini-Hochberg correction for multiple tests). Taken together, our data demonstrate that equalizing the first division results in a global increase in cell cycle pace in the P_1 lineage, leading to an altered sequence of divisions, but that this alone does not explain why some equalized embryos die whereas others do not.

We were also interested in exploring the variability of cell cycle duration in the lineaging dataset. We determined the coefficient of variation (CV) for each cell and found that the overall average CV of cell cycle duration was $4.4\% \pm 1.8$ in the wild type and $5.3\% \pm 1.8$ in *lin-5(ev571)* control embryos (Fig. 3G, $p < 0.001$), indicative of increased variability already in the latter group. In addition, we found that whereas equalized alive *lin-5(ev571)* embryos exhibited a comparable CV in cell cycle duration to control embryos ($5.2\% \pm 2.4$, $p=0.75$), it

was significantly larger in equalized dead and inverted *lin-5(ev571)* embryos, a difference due strictly to the P₁ lineage (Fig. 3G, $6.6\% \pm 2.7$ and $6.5\% \pm 4.2$, respectively, $p < 0.0001$). We conclude that equalized dead *lin-5(ev571)* embryos exhibit less stereotyped cell cycle durations.

Lineaging reveals that equalized embryos frequently exhibit defects in cell positioning and division orientation

We next report our analysis of spatial aspects in the lineaging data. In particular, we monitored cell position and division orientation along the three embryonic axes, comparing their averages to a reference model of spatially and temporally aligned control *lin-5(ev571)* embryos (Jelier et al., 2016) (Materials and Methods).

We found that equalized alive *lin-5(ev571)* embryos exhibited a mild increase in the average positional deviation per cell from the control starting at the 4-cell stage; this deviation remained essentially constant thereafter (Fig 4A, compare blue and yellow). By contrast, cell positions in equalized dead *lin-5(ev571)* embryos diverged increasingly from the control over time (Fig. 4A, compare blue and red). For inverted embryos, cell positions deviated already early on and diverged further thereafter (Fig. 4A, grey). Furthermore, we found that division orientation of individual cells exhibited a mild increase in angular deviation in equalized alive *lin-5(ev571)* embryos compared to the control, and that this deviation was more pronounced in equalized dead and inverted *lin-5(ev571)* embryos (Fig. 4B). Together, these findings establish that embryos that die following first division equalization diverge more from the norm in terms of cell positioning and division orientation than those that live.

Alterations in EMS and MS division orientation contribute to lethality of equalized embryos

Investigating spatial features in the lineaging data for individual blastomeres revealed a striking skew in the division axis of EMS at the 6-cell stage in a subset of embryos. In the wild type, the EMS spindle is oriented along the A-P axis owing to Wnt/Src signaling emanating

from P₂ (Bei et al., 2002; Liro and Rose, 2016). We found that EMS division orientation was skewed by >35° in ~19% equalized and ~43% inverted *lin-5(ev571)* embryos (Fig. 4F; n=48 and n=7). In all eight embryos with such a skew that later died, this alteration led to striking cell mispositioning at the 8-cell stage, with E and MS assuming abnormal oblique positions (Fig. 4G, top), a defect that propagated subsequently (Fig. 4G, bottom). By contrast, in the four equalized embryos that lived despite an initially aberrant EMS division angle (Fig. 4F), the skew was corrected in late anaphase, resulting in essentially normally positioned E and MS. These observations indicate that, unless corrected, a skew in the EMS division axis results in embryonic lethality.

To uncover further differences between equalized alive and equalized dead *lin-5(ev571)* embryos, excluding embryos with a T-arrangement at the 4-cell stage and those with an EMS skew at the 6-cell stage, we compared all spatial features between the two sets of embryos from the 4- to the 15-cell stage (Fig. 4 supplement A, Supplementary File 4). This analysis uncovered 10 features that differed significantly between the two groups and that were highly correlated with each other (Fig. 4 supplement A). Among these features, we found notably that the division orientation of MS deviated ~3-times more with respect to the A-P axis in equalized dead *lin-5(ev571)* embryos than in equalized alive ones (Fig. 4H). This led to increased mispositioning of the MS daughter cells MSa and MSp (Fig. 4I), which were frequently inverted along the L-R axis, a phenotype significantly associated with death (Fig. 4J-K). However, such L-R inversion was also observed in some equalized alive *lin-5(ev571)* embryos (Fig. 4I), indicating that it can be compatible with successful embryogenesis, presumably owing to subsequent compensatory movements. Taken together, these observations lead us to conclude that severe mispositioning of E and MS, as well as of MSa and MSp, can occur in equalized dead *lin-5(ev571)* embryos and contribute to lethality.

Like for the temporal data, we explored the overall variability of cell positioning and division orientation in the lineaging data set, comparing the SDs of all individual cells. As shown in Figure 4C, we found a slight increase in overall variability of cell positioning among equalized alive *lin-5(ev571)* embryos compared to the control, as well as a further significant

increase among equalized dead and inverted *lin-5(ev571)* embryos (Fig. 4D). Together, these results indicate that cell positioning and division orientation defects in equalized embryos are variable also rather than stereotyped, especially in embryos that die.

Serendipitously, we found that 6 of the 10 features identified above correlate with the extent of compression the embryo experienced from the coverslip during time-lapse imaging, suggesting that this external factor affects cell positioning, division angles and cell migration differently in equalized alive and dead *lin-5(ev571)* embryos. Furthermore, equalized dead *lin-5(ev571)* embryos tended to be significantly more compressed than equalized alive ones (Fig. 4E, $19.8 \pm 2.1 \mu\text{m}$ versus $21.9 \pm 2.2 \mu\text{m}$, $p < 0.002$), whereas a comparable degree of compression had no detrimental effect on control embryos (Fig. 4E). These observations led us to investigate directly whether equalized embryos die less frequently in the absence of compression. Therefore, we imaged uncompressed embryos using $45 \mu\text{m}$ beads or removing the coverslip after first division equalization, finding decreased lethality of equalized embryos compared to imaging under mild compressed condition with $20\text{-}25 \mu\text{m}$ beads or in the continued presence of the coverslip (33% versus 55%, $n=45$ and 174 , $p = 0.03$, Fisher's exact test). Together, these findings indicate that equalized embryos tolerate less well mechanical compression, which may perturb cell positioning, division orientation and cell-cell contacts.

Defective cell fate allocation in equalized embryos

We investigated whether defects in cell fate might occur following first division equalization, focusing our analysis on the endodermal and the pharyngeal lineages.

In the wild-type endodermal lineage, the P_1 -derived Ea/Ep cells exhibit a nearly two-fold lengthening of the cell cycle compared to the MS lineage sister cells as they ingress into the blastocoel (Fig. 5A, 5B, Sulston et al., 1983). Interestingly, we found that Ea/Ep divided earlier and ingressed less in equalized dead *lin-5(ev571)* embryos than in either control or equalized alive *lin-5(ev571)* embryos, proportionally to relative AB size (Fig. 5C-D, Fig. 5 supplement A-B, Video 8). We noted also that Ea/Ep tended to divide whilst still in contact with the eggshell in most equalized embryos (Fig. 5E, green nuclei and dashed cell contour).

Overall, we conclude that endodermal cells divide precociously and ingress only partially in equalized *lin-5(ev571)* embryos, in particular in the subset that later dies.

We set out to assess whether these alterations in Ea/Ep behavior are accompanied by improper endodermal fate specification. Normally, such specification is imparted by a redundant cascade of GATA-family transcription factors, including END-3/END-1, which peak in Ea/Ep and activate ELT-7/ELT-2, with ELT-2 remaining present throughout embryogenesis (reviewed in Maduro, 2015; McGhee, 2013). Suggestively, we found that END-3::GFP in equalized *lin-5(ev571)* embryos was expressed at lower levels than in controls ($\sim 62 \pm 19\%$, $p < 0.001$), correlating with relative AB size and Ea/Ep cell cycle duration (Fig. 5E-F; $n=18$ and $n=19$, respectively, Fig. 5 supplement C, Video 8). Furthermore, ELT-2::GFP, which is normally expressed in 8 intestinal progenitors at the ~ 100 -cell stage, was often expressed in only 2-6 cells in equalized *lin-5(ev571)* embryos (Fig. 5G-H). Together, these findings indicate that endodermal fate is acquired less faithfully following first division equalization, although altered ELT-2::GFP distribution is not significantly associated with embryonic lethality ($p=0.69$, Fisher's exact test), in line with the notion that even embryos with a partial gut can survive (Choi et al., 2017).

We also investigated fate specification of the pharyngeal lineage. In the wild type, the anterior pharynx is induced in ABalp and ABara through Delta/Notch signaling stemming from MS/MSa/MSp (reviewed in Mango, 2009). Although all four ABa descendants express the GLP-1 Notch receptor, normally ABala and ABarp are not induced since they do not contact the MS/MSa/MSp cells that express the Delta ligand (Fig. 5 supplement D). We analyzed embryos expressing the pharyngeal marker PHA-4::GFP, which is detectable at the ~ 100 -cell stage in the lineages of MS, ABalp and ABara, labeling 18 cells in total (Horner et al., 1998; Mango et al., 1994a; Murray et al., 2008). We found that equalized alive *lin-5(ev571)* embryos systematically harbored PHA-4::GFP in 18 nuclei (Fig. 5I-J; $n=5$). By contrast, abnormal PHA-4::GFP expression was observed in $\sim 47\%$ of equalized dead and inverted *lin-5(ev571)* embryos, usually with >18 positive nuclei (Fig. 5J, Fig. 5 supplement E; $n=15$). Ectopic PHA-4::GFP was present in some cells derived from ABala in 5 such embryos, and in ABarp in

another one (Fig. 5 - supplement 1E), suggesting that MS/MSa/MSp formed illegitimate contacts in these cases, leading to aberrant pharynx induction in their descendants.

Overall, we conclude that equalized *lin-5(ev571)* embryos exhibit defective fate acquisition at the least in the endodermal and pharyngeal lineages.

Viability of equalized embryos can be predicted at the 15-cell stage

We explored whether the defects thus far described occurred simultaneously in equalized embryos. However, we found no significant association between any pair of qualitative features described thus far in equalized embryos in the entire lineaging dataset (Fisher's exact test), including between additional P₄ division, EMS skew, MSa/MSp inversion, aberrant ELT-2 or PHA-4 expression, suggesting that these defects frequently arise independently of each other.

Despite such widespread phenotypic variability among equalized *lin-5(ev571)* embryos, we wondered whether the ultimate fate of equalized embryos could be predicted early in development. Again excluding embryos with a T-arrangement at the 4-cell stage or with an EMS skew at the 6-cell stage, we utilized a machine learning approach to identify a small number of features that hold predictive value for distinguishing the two sets of embryos. To this end, we utilized Lasso (Least absolute shrinkage and selection operator), which is a penalized regression method that iteratively eliminates features that contribute the least to the predictive performance of a statistical model, eventually converging on a simpler solution (Tibshirani, 1996). We conducted this analysis at the 4-, 8-, 15- and 28-cell stage, using as input all available features in each case for equalized *lin-5(ev571)* embryos (n=31 embryos scored for all features at all four stages, Supplementary File 7). To obtain a robust classifier despite the relatively small sample size, we used repeated 5-fold cross-validation, which randomly splits the data into 5 subsets of similar sizes, 4 of which are used for training the model, which is then evaluated against the remaining subset for goodness of fit. Performing 250 repetitions of cross-validation in each case, we found that features extracted at the 15-cell and 28-cell stage hold similarly high predictive value, with an overall model accuracy of $\sim 88 \pm$

438 6 % SD and $\sim 85 \pm 10$ % SD, respectively (Fig. 6A). Remarkably, we found in particular that
439 $\sim 89\%$ of the models selected at the 15-cell stage contained just 3 predictive features (Fig 6B-
440 C): ABara dorso-ventral (D-V) position, ABara positional deviation (pOV), and Ca net
441 movement (Ca.netdis). The best performing model at the 15-cell stage achieved 100%
442 sensitivity – meaning that all dead embryos were correctly classified, and 86% specificity –
443 meaning that a small fraction of alive embryos were misclassified (Fig. 6D).

444

Discussion

Asymmetric division can take several forms. In some cases, distinct fates result solely from the partitioning of cytoplasmic components asymmetrically to daughter cells of equal size. In other cases, however, asymmetric division also entails different sizes of daughter cells. Here, we uncover that *C. elegans* embryos stemming from experimentally induced equalized first division exhibit a range of incompletely penetrant phenotypic deviations from the norm (Fig. 6 – supplement 1), demonstrating that physically asymmetric division of the zygote is critical to ensure invariably successful embryogenesis.

On the importance of physically unequal asymmetric cell division

A striking example of physically unequal asymmetric division is that of the female meiotic divisions, where minute polar bodies are generated in addition to the much larger oocyte. There is little doubt that the unequal size of daughter cells is of paramount importance in this case to ensure proper allocation of maternal components to the oocyte and future embryo. Physically unequal divisions, albeit less striking in terms of size inequality, are also frequent during early embryogenesis of metazoan organisms. One possibility is that this ensures swift and proper allocation of components to daughter cells destined to yield different numbers and types of descendants in early embryos that rely on maternally contributed components and undergo rapid cell cycles. This may be particularly important in holoblastic embryos, which cleave within the constraints of an eggshell or an analogous structure, precluding compensation for potential variability in blastomere volumes through differential cell growth.

A paradigmatic example of a physically unequal division in early embryos is that of the *C. elegans* zygote, which normally yields a larger AB daughter and a smaller P₁ daughter. Previously, the specific role of size inequality had not been addressed independently from fate asymmetry. Here, we addressed this question by altering the function of the spindle positioning protein LIN-5 to equalize first cleavage without affecting A-P polarity. We discovered that first division equalization is tolerated to some extent, as evidenced by approximately half of equalized embryos completing development. Moreover, we discovered

that embryos with a relative AB size smaller than 48% always die, revealing a size asymmetry threshold for viability.

Alterations in cell cycle timing can be tolerated during *C. elegans* embryogenesis

Prior work established that the size difference between AB and P₁ contributes to their division asynchrony in the wild type, because the DNA replication checkpoint is engaged preferentially in P₁ than in AB (Brauchle et al., 2003; Stevens et al., 2016). In addition to this mechanism, the positive regulators of mitotic entry Polo-like-kinase I (PLK-1), cyclin B3 and CDC-25 phosphatase are enriched in AB compared to P₁, thereby also contributing to division asynchrony, in a size-independent manner (Budirahardja and Gönczy, 2008; Michael, 2016; Rivers et al., 2008). As anticipated from these studies, we found here that division asynchrony decreases following first division equalization, in a manner that depends on AB size. However, this asynchrony alone does not cause subsequent death, since equalized embryos with experimentally restored asynchrony die at a similar rate. This is in line with the viability of embryos lacking DNA replication checkpoint components, which also exhibit decreased asynchrony between AB and P₁ (Brauchle et al., 2003). Likewise, the majority of embryos in which asynchrony between the two cells is abrogated entirely through local infrared treatment of P₁ also live (Choi et al., 2020). Furthermore, we uncovered here that cell cycle progression is not set merely by size in all *C. elegans* embryonic blastomeres, since diminishing the size of AB and of its descendants does not slow their cell cycle, perhaps because the above mentioned positive mitotic regulators are present in excess in AB.

We found also that not only P₁, but also many of its descendants, progress faster through the cell cycle upon first division equalization. It will be interesting to address whether these later differences reflect a sustained excess of positive regulators such as PLK-1, cyclin B3 and CDC-25 inherited following first division equalization. Regardless of the underlying cause, faster cell cycle progression in the P₁ lineage might have repercussions also for fate acquisition, which can be reliant on precisely timed expression of transcription factors during *C. elegans* embryogenesis (Murray et al., 2012; Nair et al., 2013; Sarov et al., 2012).

Cell positioning, division orientation and cell fate defects upon first division equalization

Although not detrimental to viability *per se*, faster cell cycle progression in the P₁ lineage, but not in the AB lineage, results over time in an altered sequence of cell division in equalized embryos, which can lead to missing or aberrant interactions between cells. A particularly striking example occurs in a minor fraction of equalized embryos that exhibit an aberrant T-arrangement at the 4-cell stage, leading to a lack of inductive Delta/Notch signaling. Suggestively, we found that equalized embryos with such a T-arrangement tend to be elongated (see legend of Fig. 2 – supplement 1). Compatible with embryo length playing a role, T-arrangements also occur in *lon-1* mutant embryos, which are very elongated but where AB and P₁ have normal relative sizes (Yamamoto and Kimura, 2017). Interestingly, a similar T-arrangement occurs naturally in other Nematode clades, reflecting plasticity in early division patterns that likely requires adaptations of fate determination networks (Brauchle et al., 2009; Schulze and Schierenberg, 2011, 2009).

Missing or aberrant interactions between cells can also derive from defective division orientation, leading to daughter cell mispositioning, as exemplified with the skewed EMS and MS division orientation. Interestingly, an EMS skew is observed also upon impaired Wnt signaling from P₂ (Bei et al., 2002; Schlesinger et al., 1999; Thorpe et al., 1997). More generally, a posterior signaling center that relies on a Wnt-dependent relay mechanism originating from P₂/P₃ polarizes multiple cells during *C. elegans* embryogenesis (Bischoff and Schnabel, 2006), and our findings are compatible with the possibility that this signaling center is compromised upon first cleavage equalization. Furthermore, the EMS skew might affect cell-cell contacts and therefore alter the instructive Delta/Notch signaling that normally occurs between MS and two adjacent ABa-derived cells, which are thereby triggered to differentiate towards pharyngeal fates (reviewed in Mango, 2009). We indeed observed inappropriate induction of pharyngeal fate in several ABa cells, raising the possibility that aberrant contacts occurred between MS/MSa/MSp, which express a Delta ligand, and ABa or ABap, which express a Notch receptor, but that are normally shielded from ligand binding owing to their

distant location. Moreover, we noted that the intestinal progenitors Ea/Ep expressed less END-3::GFP in equalized embryos, perhaps reflecting insufficient induction by maternal factors, followed by stochastic expression of the downstream component ELT-2. Compatible with this view, maternally provided SKN-1, as well as its targets END-1 and END-3, must reach a critical threshold for complete activation of ELT-2 (Maduro, 2015; Raj et al., 2010).

Regarding MS position, a physical computational model predicted that abolishing both size asymmetry and asynchrony between AB and P₁ lineages would impact the positions of MS and E daughters at the 24-cell stage in ~25% of embryos (Fickentscher et al., 2016). Accordingly, we observed instances of MSa/MSp mispositioning and incomplete ingression of E daughters in equalized *lin-5(ev571)* embryos. Thus, these defects in equalized embryos could be at least in part explained based on force balance among cells with altered volumes and division timing.

Detailed lineage analysis enabled us to uncover that in many equalized embryos the germline progenitor P₄ undergoes continued divisions in a manner that resembles the behavior of its cousin D. Such a defect in germline fate specification could help explain the reduced fertility observed in some adults that derive from embryos that survived equalization. Lineage transformation of P₄ into D also occurs in embryos derived from *mes-1* mutant animals, in which P₂ and P₃ lack proper polarity (Berkowitz and Strome, 2000). By extension, such polarity defects may also be present following first division equalization. In the wild type, P₄ divides symmetrically and its daughters remain quiescent until hatching (Sulston et al., 1983). A size dependent switch from asymmetric to symmetric division occurs in P₄ as it reaches a size too small to allow formation of the reciprocal PAR protein gradient (Hubatsch et al., 2019). Our findings lead us to speculate that P₄ cell size reduction might be required not only for this switch of division mode, but also to maintain germ line progenitors quiescent until hatching.

Physically asymmetric division of the *C. elegans* zygote ensures invariably successful embryonic development

Wild-type *C. elegans* embryogenesis is highly stereotyped, exhibiting little variability between embryos in terms of division timing, cell positioning, division orientation and fate acquisition, ultimately yielding 558 cells at hatching in the hermaphrodite (Richards et al., 2013; Sulston et al., 1983). The array of incompletely penetrant and variable defects revealed here implies that a physically unequal first division is critical for the stereotypy of *C. elegans* embryogenesis.

Despite important phenotypic variability upon first division equalization, we found that three features at the 15-cell stage together hold strong predictive power in predicting the ultimate fate of equalized embryos: ABar D-V position, ABar positional deviation, and Ca net displacement. Closer analysis of cell positions in the lineaging data set lends further support to the importance of these three features. Indeed, several AB descendants on the right side of embryo, including ABar and its progeny, were significantly shifted dorsally as early as the 8-cell stage solely in dying embryos (Fig. 6 – supplement 2, Supplementary File 2). Although the mechanisms responsible for such dorsally shifted position or for increased Ca movement in equalized dead *lin-5(ev571)* embryos remain to be fully understood, we conclude that these three features provide a shared early signature amongst most equalized embryos that then diverges into more variable phenotypic manifestations.

We also wondered whether having differently sized AB and P₁ blastomeres contributes to robust embryogenesis. Developmental systems are deemed to be robust if they remain unchanged or else change in a reproducible manner in the face of a given perturbation. The loss of robustness is manifested by increased variability upon perturbation without a change in the mean (reviewed in Félix and Barkoulas, 2015). Applying these criteria to features monitored in our data set, we found only 23 of the 1608 analyzed in which the mean remained the same but the variability increased when comparing equalized *lin-5(ev571)* and control embryos (Figure 6 – supplemental figure 3). This indicates that these features in particular are less robust to perturbation by first division equalization. Moreover, our findings suggest that

having differently sized AB and P₁ blastomeres provides resilience against mechanical stress, as evidenced by the increased lethality of equalized *lin-5(ev571)* embryos upon compression. Normally, compressed *C. elegans* embryos can correct specific defects in cell positioning through the concerted migration of several AB descendants (Jelier et al., 2016). Presumably compressed equalized embryos cannot undertake such corrective movements for steric reasons or because their fate is compromised.

How general is the importance of having differently sized blastomeres in early embryogenesis? Physically asymmetric cleavage of the zygote is present across the Rhabditida order (Brauchle et al., 2009; Valfort et al., 2018), suggesting functional importance over substantial evolutionary times. Moreover, unequal cleavages are present in early development of other systems, including annelid, ascidian and echinoderm embryos (reviewed in Moorhouse and Burgess, 2014; Negishi and Nishida, 2017; Shimizu et al., 1998). Conversely, generating cells of equal sizes seems of importance during early human development, since unevenly sized blastomeres frequently correlate with aneuploidy and lower rates of implantation and pregnancy (Hardarson et al., 2001). Overall, generating appropriately proportioned daughter cells is widespread in metazoan organisms, and our work demonstrates the importance of physical asymmetry of the first division in *C. elegans*, which is fundamental for ensuring invariably successful development.

Acknowledgements

We are grateful to Zoltan Spiró for his initial observation of acute temperature sensitivity of *lin-5(ev571)*, as well as to Sander van den Heuvel, Joel Rothman and Geraldine Seydoux for their generous sharing of strains. Some strains were provided by the Caenorhabditis Genetics Center (CGC), which is funded by the NIH Office of Research Infrastructure Programs (P40 OD010440). We thank Alessandro Berto, Alexandra Bezler, Nils Kalbfus and Fabian Schneider for constructive comments on the manuscript, as well as Marco Mina for advice on statistics. For help with image acquisition and processing, we thank Olivier Burri and Nicolas

Chiaruttini from the Bioimaging and Optics platform of the School of Life Sciences (EPFL, Lausanne).

Materials and methods

C. elegans strains and embryo preparation

C. elegans strains used in this study are listed in Supplementary File 5 and were maintained on standard NGM plates with OP50 *Escherichia coli* as a food source. Temperature-sensitive strains were maintained at 16°C, other strains at 20°C. Strains expressing the desired fluorescent markers were crossed with *lin-5(ev571)* carrying strain and homozygous progeny was selected based on temperature sensitivity and fluorescent marker expression. After establishing a given strain, worms were maintained for at least one generation prior to analysis. For embryo imaging, 1-2 day old adult *lin-5(ev571)* hermaphrodites were dissected in M9 buffer chilled at 15°C, and one-cell stage embryos with visible pronuclei collected using a mouth pipet. Embryos were then mounted either on a 2% agarose pad for DIC imaging with oil immersion objectives, or into a bead slurry containing 20 µm polystyrene beads (Polysciences - #18329-5) in M9 + 0.5% (w/v) methylcellulose for water immersion objectives or 20% iodixanol (Optiprep, Sigma Aldrich) for glycerol objectives to raise the refractive index of the medium (Boothe et al., 2017). Two methods were utilized to image embryos without compression. First, we mounted embryos in a viscous M9 medium containing + 0.5% (w/v) methylcellulose and 45 µm polystyrene beads. Second, embryos were mounted on a 2% agarose pad as usual, but the coverslip removed after the temperature shift, and the embryo then deposited with the pad onto an NGM plate. Non-compressed embryos obtained by either method were analyzed for the extent of embryonic lethality.

Temperature shift for size equalization

Rapid temperature shifts between 17°C and 27°C were performed on the microscope stage with the CherryTemp fluidic temperature controller (Cherry Biotech, France). The CherryTemp device is equipped with two thermalization chambers that were set to 17°C and 27°C. By

changing the chamber through which the thermalization solution flowed, the sample was rapidly (~15 s) shifted to the desired temperature. To generate equally dividing *lin-5(ev571)* one-cell stage embryos, we performed the upshift right after NEBD for embryos imaged by DIC and at metaphase for embryos expressing fluorescently labeled histone, and kept them at the restrictive temperature of 27°C until the completion of cytokinesis, ~5 min thereafter. Thereafter, the sample was shifted back to the permissive temperature of 17°C for the rest of embryogenesis. Embryos imaged only for a fraction of embryogenesis were moved to an incubator set to 17°C and survival scored the next day. In all experiments, we scored as “alive” embryos that reached a normal looking, motile, 3-fold pre-larval stage, or that hatched, and as “dead” embryos with an abnormal morphology at that stage or unable to hatch. Note that the *lin-5(ev571)* strain used for the majority of experiments expressed in addition the plasma membrane marker GFP::PH and the chromatin marker mCherry::H2B; this strain exhibited a lethality on plates of 4.7% (n=829), close to that of *lin-5(ev571)* embryos (2.5%, n=394).

Time-lapse microscopy

DIC time-lapse microscopy was performed on a Zeiss Axioscope 2 equipped with DIC optics and a 100x 1.25 NA Achrostat objective, recording with a USB3.0 1.3MP monochrome CMOS camera (Ximea - model MQ013MG-E2, Slovakia), controlled by the open-source µManager software (Edelstein et al., 2014).

Combined DIC and epifluorescence time-lapse microscopy was performed on a motorized Zeiss Axio Observer D1 using a 63x 1.2 NA C-Apochromat water immersion objective, equipped with an Andor Zyla 4.2 sCMOS camera, a piezo controlled Z-stage (Ludl Electronic Products), and an LED light source (Lumencor SOLA II). The setup was controlled by µManager.

The lineaging dataset was acquired on a Leica SP8 laser scanning confocal microscope equipped with a 60x HC PL APO 1.3 NA glycerol immersion objective, HyD detectors set to 100% sensitivity, and a tunable Chameleon laser (Coherent). Time-lapse recordings were

acquired at 2.5 min intervals, capturing 35 slices 0.75 μ apart, typically for 100 frames. The microscope was set to 8kHz resonance scanning mode to reduce phototoxicity (Richards et al., 2013), 4 x line averaging plus 2 x frame accumulation, with a pixel size of 140 nm, a pixel dwell time of 50-70 ns, and the pinhole set to 1.2 Airy units. To compensate for the signal loss deeper in the sample, the excitation light was ramped across the Z range from 2 \rightarrow 15% for the 488 nm laser line and from 2 \rightarrow 18% for the 585 nm laser line. Embryos were mounted in M9-20% iodixanol (Optiprep – Sigma Aldrich) to match the sample's refractive index (Boothe et al., 2017), and placed in a sandwich between two #1.5 coverslips (40x22 mm and 18x18 mm) separated by 20 μ m polystyrene beads and sealed with melted VALAP (vaseline, lanolin, paraffin, 1:1:1). Sample temperature was maintained at 17°C using the CherryTemp temperature controller. The coverslip sample sandwich was attached to the CherryTemp thermalization chip glass surface through a thin layer of water.

Optogenetic-mediated division equalization

Worms expressing LIN-5::EPDZ::mCherry, PH::EGFP::LOV and GFP::TBB-2 in the embryo (a kind gift from Sander van den Heuvel) were dissected in a dark room under a red light to prevent premature activation of PH::LOV, and mounted for imaging on 2% agarose pads (Fielmich et al., 2018). Imaging was performed on a Leica SP8 in the Live Data Mode of the LAS X software, allowing to toggle laser lines on/off during acquisition. The microscope settings were the same as above with the following modifications: no Z-compensation of exposure, time-lapse acquired at 10s interval, capturing 11 slices with 1.25 μ m spacing, and this for 80-100 frames (from 1- to 4-cell stage); moreover, the temperature was maintained at 22°C. LIN-5::EPDZ::mCherry distribution was monitored with a 585 nm laser; 585 nm transmitted light images were collected on an additional PMT detector to follow NEBD for analysis of AB/P₁ mitotic asynchrony. Interaction of LIN-5::LOV with PH::EPDZ was induced by activating the 488 nm laser at 3-5% intensity only during acquisition in a small rectangular region (~10x5 μ m) at the anterior cortex, from NEBD until cytokinesis completion.

Cell cycle retardation with 405 nm laser

A pulsed 405 nm diode laser (at 70% output, 700 milliwatts/cm² at 100%) was continuously scanned over the entire P₁ nucleus early in the 2-cell stage for 4.5 minutes at 8 kHz, using a 70 ns dwell time on the SP8 confocal setup described above. This induces photodamage, likely in the form of thymidine dimers in the DNA, which might cause replication fork stalling and activation of the DNA replication checkpoint. Using otherwise wild-type embryos expressing mCherry::H2B, we determined experimentally an optimal non-lethal duration (4.5 min) of continuous laser scanning that induces enhances the delay between AB and P₁ mitoses from the normal $\sim 3.5 \pm 0.34$ minutes to $\sim 6 \pm 1.6$ minutes at 17°C.

Image processing and analysis

All images were rotated, Z-projected and adjusted in Fiji (ImageJ) for display (Schindelin et al., 2012). The 2D surface of the AB and P₁ cells was determined manually from DIC images, or from the GFP::PH plasma membrane signal in strains expressing this marker. This was achieved by tracing cell outlines with a Fiji polygon tool at the mid-plane, with both nuclei in focus, when the interface between AB and P₁ was perfectly straight, ~ 5 minutes after cytokinesis. The size of AB was then expressed relative to the embryo cross-sectional area, corresponding to the sum of the P₁ and AB surfaces. To assess how well the 2D mid-plane cell area measurements matched the corresponding 3D cell volumes, we analyzed embryos expressing GFP::PH, segmenting the full 3D volumes of AB and P₁ using a watershed-based segmentation (MorphoLibJ plugin in Fiji).

Analysis of marker gene expression

Embryos expressing endogenously tagged PAR-2::GFP and mCherry::MEX-5 were imaged on a wide-field Zeiss Axio-Observer microscope as described above. Images were taken every 30 seconds until the 4-cell stage, capturing 11 planes with 1.5 μ m spacing. For signal quantification, we determined the mean intensity in the mid-plane at the two-cell stage, including the area covering the nucleus and the entire cortex. MEX-5 intensity was normalized

to the mean AB intensity in control embryos from the corresponding day because MEX-5 intensity differed significantly between experiments.

Transgenic embryos expressing END-3::GFP or ELT-2::GFP in a *lin-5(ev571)* background were imaged using combined DIC and fluorescence time-lapse microscopy as described above, with two-minute intervals and 1 μ m optical slicing, capturing a 25 μ m stack. Gastrulation movements of Ea/Ep cells were tracked in 3D with the TrackMate Fiji plugin (Tinevez et al., 2017), utilizing the nuclear END-3::GFP signal, which is expressed from the beginning of the Ea/Ep cell cycle (Maduro et al., 2005). We then quantified the peak GFP intensity, i.e., the mean voxel intensity in the nuclear volume obtained from the sphere detection macro in TrackMate. The ELT-2::GFP expression pattern was scored visually for the number of GFP positive cells at the E8 stage. Analysis of pharyngeal differentiation was based on the PHA-4::GFP expression pattern in embryos co-expressing the pan-nuclear mCherry::H2B marker (Sarov et al., 2012). Embryos were imaged with the SP8 confocal microscope as described above followed by cell lineaging as described below, allowing us to determine the identity of GFP positive cells at the ~100-cell stage.

Statistics and data analysis

Box and whisker plots shown throughout this manuscript were generated in R using the boxplot function. Briefly, each box contains 50% of all data points between the first and third quartile (IQR – inter-quartile range) and its center lies at the mean along the Y-axis, with the median indicated by a thick line in the box. Whiskers extend to $\pm 1.58 \text{ IQR}/\sqrt{n}$. Data points out of this range are shown as individual points and can be considered as outliers, except for plots of variability, where outliers are not displayed for simplicity.

Statistical comparisons were performed in R using Welch's two sample t-test with Benjamini-Hochberg correction for multiple comparisons unless indicated otherwise in the figure legends. Simultaneous comparisons of multiple groups for difference in their means were performed using Tukey's honest significant difference test.

Lineage tracing

3D time-lapse recordings of embryos expressing mCherry::H2B in either wild-type or *lin-5(ev571)* background were first pre-processed to enhance the nuclear signal and remove noise with the Noise2Void/CARE machine learning pipeline (Krull et al., 2019). Thereafter, a custom Fiji macro was used to correct the drift using the first polar body as a bright fiducial marker. The lineage was then traced using a level-set image segmentation and model evolution implemented in MATLAB (MathWorks, USA) as described previously (Dzyubachyk et al., 2010; Krüger et al., 2015), and corrected in the WormDeLux Java-based lineage editor (Jelier et al., 2016). Results were exported in the StarryNite format (Bao and Murray, 2011). Cells were then automatically named in the lineage editor according to the canonical lineage (Sulston et al., 1983), and manually checked afterward for possible errors, especially in mutant embryos that often substantially deviated in division orientation and cell positioning from the wild-type model used for naming.

As mentioned also in the results section, all lineage files and the source code are available at <https://github.com/UPGON/worm-rules-eLife>. Note that we excluded embryos with the 4-cell stage T-arrangement from the lineage analysis because they are known to exhibit specific defects stemming from the lack of ABp induction (Priess and Thomson, 1987), which would introduce additional variability and thus mask potential novel phenotypes. Note that some embryos were imaged only up to the 26-cell stage; therefore, the number of embryos used for statistical comparison differs for individual cells and in different analyses reported in this manuscript; Supplementary File 2 reports the number of embryos/cells used for each comparison.

Data analysis of lineaged embryos

Lineages in the StarryNite format were imported into R version 3.6.1 (R Core Team, 2014). The growth curves of all embryos were aligned in time and a specific scaling factor for each embryo was deployed to match the mean pace of wild-type development at 17°C based on the maximum correlation between the wild type and each experimental curve

(Supplementary File 1). Differential pace of development could be caused by slight variations in temperature or by inherent embryo variability. We then set ABa division time as time 0 because time-lapse recording for the lineaging experiments typically started at the 4-cell stage, after the temperature upshift was performed during the first division or in the early 2-cell stage for controls.

Embryos were aligned in space with respect to their inferred anterior-posterior (A-P) and dorso-ventral (D-V) axes using a custom Java-based script (Jelier et al., 2016). First, nuclear positions were normalized to length, width, and height of each embryo along each imaging axis. Then, the alignment method first determines the A-P axis coinciding with the first principal component of the PCA calculated from all nuclear positions within first 100 frames of development. The D-V axis is orthogonal to the A-P axis and proceeds through the ventral surface of the embryo defined as the average position of the MS lineage cells. Finally, the left-right (L-R) axis is orthogonal to both the A-P and D-V axes.

Feature extraction

We then computed 13 features (variables) using this aligned dataset for each cell in every embryo. First, we computed the time of cell birth (variable name (v): StartTime), and cell cycle duration (v: LifeTime), as well as the time of division (v: EndTime). Next, we recorded 3D positions of each cell along the three principal axes at the last frame before anaphase (variables: pAP, pLR, pDV), as well as the total trajectory distance (totdis) and the net displacement (netdis) of each cell as the Euclidian distance between nuclear 3D coordinates at birth and at the end of the cell cycle. Further, division angles (v: aAP, aLR, aDV) were computed with respect to the inferred embryonic axes at the first frame after anaphase onset. The last two variables, i.e. angular (v: aMean) and positional deviation (v: pOV), required a comparison of a given embryo to the *lin-5(ev571)* control model that was determined by aligning embryos in time and space using the General Procrustes Analysis (Gower, 1975) and then calculating average positions of individual cells. Using this model, overall angular deviation (v: aMean) was computed as an angle between the reference division vector and the

observed spindle orientation vector in a given embryo for each cell (Jelier et al., 2016). Similarly, positional deviation was calculated as the Euclidean distance between the position of a given nucleus at metaphase from that in the control model. Supplementary File 2 contains complete statistics for all 13 features in experimental groups of embryos.

Variable filtering and intra-group variation

We filtered variables according to effect size and statistical significance comparing equalized dead and alive *lin-5(ev571)* embryos at the 15-cell stage. We chose an arbitrary effect threshold of 15% and calculated Welch's unequal variances t-test for each variable. The p-value cut-off $\alpha = 0.008$ was determined for a false discovery rate of 10% using scrambled experimental data with shuffled group labels (100 repetitions). We then plotted effect size versus p-value as a volcano plot.

To assess variability within each group of embryos, we calculated the standard deviation and the coefficient of variation (CV) for each cell and every feature. In particular, the CV was used to compare cell cycle variability among different cells that have lineage and stage-specific differences in average cell cycle duration. To assess the mean and the variance (Figure 6 – supplement 3), we required each feature to be scored in at least 5 embryos in both alive and dead equalized groups, thereby decreasing the total number of analyzed features to 1608.

Predictive model of developmental outcome using Lasso

We searched the parameter space of variables at 4-, 8-, 15-, and 28-cell stage for features that would predict lethality in equalized embryos (n=31 embryos scored for all features at all these stages). Data preprocessing before feeding data into the model building pipeline included removing those variables with low overall variance (empirically set at <2.5%, n=24 variables), those that would have more than 25% of missing value (n=12 variables), and also replacing missing values with the group mean (128/19158 values), and scaling each variable within a 0-1 range. We used the penalized Lasso regression to generate a binary classification model (glmnet R package). We employed a machine learning strategy to obtain a robust value

818 of the shrinkage coefficient λ by performing 5-fold cross-validation (CV) 250 - times and
819 choosing a model with minimal cross-validation mean squared error. We report average
820 classification accuracy for best models selected over 250 CV iterations. To evaluate the
821 stability of solutions thus obtained, we scored the number of chosen predictors and their
822 identity over 250 iterations.

823 References

- 824 Bao Z, Murray JI. 2011. Mounting *Caenorhabditis elegans* Embryos for Live Imaging of
825 Embryogenesis. *Cold Spring Harb Protoc* **2011**:pdb.prot065599.
826 doi:10.1101/pdb.prot065599
- 827 Bao Z, Murray JI, Boyle T, Ooi SL, Sandel MJ, Waterston RH. 2006. Automated cell lineage
828 tracing in *Caenorhabditis elegans*. *Proc Natl Acad Sci U S A* **103**:2707–2712.
829 doi:10.1073/pnas.0511111103
- 830 Bei Y, Hogan J, Berkowitz LA, Soto M, Rocheleau CE, Pang KM, Collins J, Mello CC. 2002.
831 SRC-1 and Wnt Signaling Act Together to Specify Endoderm and to Control Cleavage
832 Orientation in Early *C. elegans* Embryos. *Dev Cell* **3**:113–125. doi:10.1016/S1534-
833 5807(02)00185-5
- 834 Berkowitz LA, Strome S. 2000. MES-1, a protein required for unequal divisions of the germline
835 in early *C. elegans* embryos, resembles receptor tyrosine kinases and is localized to
836 the boundary between the germline and gut cells. *Development* **127**:4419–4431.
- 837 Bischoff M, Schnabel R. 2006. A Posterior Centre Establishes and Maintains Polarity of the
838 *Caenorhabditis elegans* Embryo by a Wnt-Dependent Relay Mechanism. *PLOS Biol*
839 **4**:e396. doi:10.1371/journal.pbio.0040396
- 840 Boothe T, Hilbert L, Heide M, Berninger L, Huttner WB, Zaburdaev V, Vastenhouw NL, Myers
841 EW, Drechsel DN, Rink JC. 2017. A tunable refractive index matching medium for live
842 imaging cells, tissues and model organisms. *eLife* **6**:e27240. doi:10.7554/eLife.27240
- 843 Brauchle M, Baumer K, Gönczy P. 2003. Differential Activation of the DNA Replication
844 Checkpoint Contributes to Asynchrony of Cell Division in *C. elegans* Embryos. *Curr*
845 *Biol* **13**:819–827. doi:10.1016/S0960-9822(03)00295-1
- 846 Brauchle M, Kiontke K, MacMenamin P, Fitch DHA, Piano F. 2009. Evolution of early
847 embryogenesis in rhabditid nematodes. *Dev Biol* **335**:253–262.
848 doi:10.1016/j.ydbio.2009.07.033
- 849 Budirahardja Y, Gönczy P. 2008. PLK-1 asymmetry contributes to asynchronous cell division
850 of *C. elegans* embryos. *Development* **135**:1303–1313. doi:10.1242/dev.019075
- 851 Cabernard C, Doe CQ. 2009. Apical/Basal Spindle Orientation Is Required for Neuroblast
852 Homeostasis and Neuronal Differentiation in *Drosophila*. *Dev Cell* **17**:134–141.
853 doi:10.1016/j.devcel.2009.06.009
- 854 Choi H, Broitman-Maduro G, Maduro MF. 2017. Partially compromised specification causes
855 stochastic effects on gut development in *C. elegans*. *Dev Biol* **427**:49–60.
856 doi:10.1016/j.ydbio.2017.05.007
- 857 Choi J, Zhou H, Landig R, Wu H-Y, Yu X, Stetina SEV, Kucsko G, Mango SE, Needleman DJ,
858 Samuel ADT, Maurer PC, Park H, Lukin MD. 2020. Probing and manipulating
859 embryogenesis via nanoscale thermometry and temperature control. *Proc Natl Acad*
860 *Sci*. doi:10.1073/pnas.1922730117
- 861 Colombo K, Grill SW, Kimple RJ, Willard FS, Siderovski DP, Gönczy P. 2003. Translation of
862 Polarity Cues into Asymmetric Spindle Positioning in *Caenorhabditis elegans*
863 Embryos. *Science* **300**:1957–1961. doi:10.1126/science.1084146
- 864 Cuenca AA, Schetter A, Aceto D, Kempfues K, Seydoux G. 2003. Polarization of the *C.*
865 *elegans* zygote proceeds via distinct establishment and maintenance phases. *Dev*
866 *Camb Engl* **130**:1255–1265. doi:10.1242/dev.00284
- 867 Dzyubachyk O, van Cappellen WA, Essers J, Niessen WJ, Meijering E. 2010. Advanced
868 Level-Set-Based Cell Tracking in Time-Lapse Fluorescence Microscopy. *IEEE Trans*
869 *Med Imaging* **29**:852–867. doi:10.1109/TMI.2009.2038693
- 870 Félix M-A, Barkoulas M. 2015. Pervasive robustness in biological systems. *Nat Rev Genet*
871 **16**:483–496. doi:10.1038/nrg3949
- 872 Fickentscher R, Struntz P, Weiss M. 2016. Setting the Clock for Fail-Safe Early
873 Embryogenesis. *Phys Rev Lett* **117**:188101. doi:10.1103/PhysRevLett.117.188101
- 874 Fielmich L-E, Schmidt R, Dickinson DJ, Goldstein B, Akhmanova A, van den Heuvel S. 2018.
875 Optogenetic dissection of mitotic spindle positioning in vivo. *eLife* **7**.
876 doi:10.7554/eLife.38198

- Fisk Green R, Lorson M, Walhout AJM, Vidal M, van den Heuvel S. 2004. Identification of critical domains and putative partners for the *Caenorhabditis elegans* spindle component LIN-5. *Mol Genet Genomics MGG* **271**:532–544. doi:10.1007/s00438-004-1012-x
- Goldstein B, Hird SN. 1996. Specification of the anteroposterior axis in *Caenorhabditis elegans*. *Development* **122**:1467–1474.
- Goldstein B, Nance J. 2020. *Caenorhabditis elegans* Gastrulation: A Model for Understanding How Cells Polarize, Change Shape, and Journey Toward the Center of an Embryo. *Genetics* **214**:265–277. doi:10.1534/genetics.119.300240
- Gotta M, Ahringer J. 2001. Distinct roles for G α and G $\beta\gamma$ in regulating spindle position and orientation in *Caenorhabditis elegans* embryos. *Nat Cell Biol* **3**:297–300. doi:10.1038/35060092
- Gotta M, Dong Y, Peterson YK, Lanier SM, Ahringer J. 2003. Asymmetrically Distributed C. *elegans* Homologs of AGS3/PINS Control Spindle Position in the Early Embryo. *Curr Biol* **13**:1029–1037. doi:10.1016/S0960-9822(03)00371-3
- Gower JC. 1975. Generalized procrustes analysis. *Psychometrika* **40**:33–51. doi:10.1007/BF02291478
- Grill SW, Gönczy P, Stelzer EHK, Hyman AA. 2001. Polarity controls forces governing asymmetric spindle positioning in the *Caenorhabditis elegans* embryo. *Nature* **409**:630–633. doi:10.1038/35054572
- Grill SW, Howard J, Schäffer E, Stelzer EHK, Hyman AA. 2003. The Distribution of Active Force Generators Controls Mitotic Spindle Position. *Science* **301**:518–521. doi:10.1126/science.1086560
- Hardarson T, Hanson C, Sjögren A, Lundin K. 2001. Human embryos with unevenly sized blastomeres have lower pregnancy and implantation rates: indications for aneuploidy and multinucleation. *Hum Reprod Oxf Engl* **16**:313–318. doi:10.1093/humrep/16.2.313
- Horner MA, Quintin S, Domeier ME, Kimble J, Labouesse M, Mango SE. 1998. pha-4, an HNF-3 homolog, specifies pharyngeal organ identity in *Caenorhabditis elegans*. *Genes Dev* **12**:1947–1952.
- Hubatsch L, Peglion F, Reich JD, Rodrigues NTL, Hirani N, Illukkumbura R, Goehring NW. 2019. A cell-size threshold limits cell polarity and asymmetric division potential. *Nat Phys* **15**:1–8. doi:10.1038/s41567-019-0601-x
- Jelier R, Kruger A, Swoger J, Zimmermann T, Lehner B. 2016. Compensatory Cell Movements Confer Robustness to Mechanical Deformation during Embryonic Development. *Cell Syst* **3**:160–171. doi:10.1016/j.cels.2016.07.005
- Kemphues KJ, Priess JR, Morton DG, Cheng N. 1988. Identification of genes required for cytoplasmic localization in early C. *elegans* embryos. *Cell* **52**:311–320. doi:10.1016/S0092-8674(88)80024-2
- Kemphues KJ, Strome S. 1997. Fertilization and Establishment of Polarity in the Embryo In: Riddle DL, Blumenthal T, Meyer BJ, Priess JR, editors. C. *Elegans* II. Cold Spring Harbor (NY): Cold Spring Harbor Laboratory Press.
- Kiontke K, Fitch DHA. 2005. The phylogenetic relationships of *Caenorhabditis* and other rhabditids. *WormBook*. doi:10.1895/wormbook.1.11.1
- Kiontke KC, Félix M-A, Ailion M, Rockman MV, Braendle C, Pénigault J-B, Fitch DH. 2011. A phylogeny and molecular barcodes for *Caenorhabditis*, with numerous new species from rotting fruits. *BMC Evol Biol* **11**:339. doi:10.1186/1471-2148-11-339
- Kitajima A, Fuse N, Isshiki T, Matsuzaki F. 2010. Progenitor properties of symmetrically dividing *Drosophila* neuroblasts during embryonic and larval development. *Dev Biol* **347**:9–23. doi:10.1016/j.ydbio.2010.06.029
- Kotak S, Gönczy P. 2013. Mechanisms of spindle positioning: cortical force generators in the limelight. *Curr Opin Cell Biol, Cell cycle, differentiation and disease* **25**:741–748. doi:10.1016/j.ceb.2013.07.008
- Krüger AV, Jelier R, Dzyubachyk O, Zimmermann T, Meijering E, Lehner B. 2015. Comprehensive single cell-resolution analysis of the role of chromatin regulators in early C. *elegans* embryogenesis. *Dev Biol* **398**:153–162. doi:10.1016/j.ydbio.2014.10.014

- Krull A, Vicar T, Jug F. 2019. Probabilistic Noise2Void: Unsupervised Content-Aware Denoising. *ArXiv190600651 Cs Eess*.
- Lee J-Y, Marston DJ, Walston T, Hardin J, Halberstadt A, Goldstein B. 2006. Wnt/Frizzled Signaling Controls C. elegans Gastrulation by Activating Actomyosin Contractility. *Curr Biol* **16**:1986–1997. doi:10.1016/j.cub.2006.08.090
- Liro MJ, Rose LS. 2016. Mitotic Spindle Positioning in the EMS Cell of Caenorhabditis elegans Requires LET-99 and LIN-5/NuMA. *Genetics* **204**:1177–1189. doi:10.1534/genetics.116.192831
- Lorson MA, Horvitz HR, van den Heuvel S. 2000. LIN-5 is a novel component of the spindle apparatus required for chromosome segregation and cleavage plane specification in Caenorhabditis elegans. *J Cell Biol* **148**:73–86.
- Maduro MF. 2015. Developmental robustness in the Caenorhabditis elegans embryo. *Mol Reprod Dev* **82**:918–931. doi:10.1002/mrd.22582
- Maduro MF, Hill RJ, Heid PJ, Newman-Smith ED, Zhu J, Priess JR, Rothman JH. 2005. Genetic redundancy in endoderm specification within the genus Caenorhabditis. *Dev Biol* **284**:509–522. doi:10.1016/j.ydbio.2005.05.016
- Mango SE. 2009. The molecular basis of organ formation: insights from the C. elegans foregut. *Annu Rev Cell Dev Biol* **25**:597–628. doi:10.1146/annurev.cellbio.24.110707.175411
- Mango SE, Lambie EJ, Kimble J. 1994a. The pha-4 gene is required to generate the pharyngeal primordium of Caenorhabditis elegans. *Development* **120**:3019–3031.
- Mango SE, Thorpe CJ, Martin PR, Chamberlain SH, Bowerman B. 1994b. Two maternal genes, apx-1 and pie-1, are required to distinguish the fates of equivalent blastomeres in the early Caenorhabditis elegans embryo. *Development* **120**:2305–2315.
- McGhee JD. 2013. The Caenorhabditis elegans intestine. *Wiley Interdiscip Rev Dev Biol* **2**:347–367. doi:10.1002/wdev.93
- Mello CC, Draper BW, Priess JR. 1994. The maternal genes apx-1 and glp-1 and establishment of dorsal-ventral polarity in the early C. elegans embryo. *Cell* **77**:95–106. doi:10.1016/0092-8674(94)90238-0
- Michael WM. 2016. Cyclin CYB-3 controls both S-phase and mitosis and is asymmetrically distributed in the early C. elegans embryo. *Development* **143**:3119–3127. doi:10.1242/dev.141226
- Moorhouse KS, Burgess DR. 2014. How to be at the right place at the right time: the importance of spindle positioning in embryos. *Mol Reprod Dev* **81**:884–895. doi:10.1002/mrd.22418
- Munro E, Nance J, Priess JR. 2004. Cortical Flows Powered by Asymmetrical Contraction Transport PAR Proteins to Establish and Maintain Anterior-Posterior Polarity in the Early C. elegans Embryo. *Dev Cell* **7**:413–424. doi:10.1016/j.devcel.2004.08.001
- Murray JI, Bao Z, Boyle TJ, Boeck ME, Mericle BL, Nicholas TJ, Zhao Z, Sandel MJ, Waterston RH. 2008. Automated analysis of embryonic gene expression with cellular resolution in C. elegans. *Nat Methods* **5**:703–709. doi:10.1038/nmeth.1228
- Murray JI, Boyle TJ, Preston E, Vafeados D, Mericle B, Weisdepp P, Zhao Z, Bao Z, Boeck M, Waterston RH. 2012. Multidimensional regulation of gene expression in the C. elegans embryo. *Genome Res* **22**:1282–1294. doi:10.1101/gr.131920.111
- Nair G, Walton T, Murray JI, Raj A. 2013. Gene transcription is coordinated with, but not dependent on, cell divisions during C. elegans embryonic fate specification. *Development* **140**:3385–3394. doi:10.1242/dev.098012
- Negishi T, Nishida H. 2017. Asymmetric and Unequal Cell Divisions in Ascidian Embryos. *Results Probl Cell Differ* **61**:261–284. doi:10.1007/978-3-319-53150-2_12
- Ou G, Stuurman N, D'Ambrosio M, Vale RD. 2010. Polarized Myosin Produces Unequal-Size Daughters During Asymmetric Cell Division. *Science* **330**:677–680. doi:10.1126/science.1196112
- Park DH, Rose LS. 2008. Dynamic localization of LIN-5 and GPR-1/2 to cortical force generation domains during spindle positioning. *Dev Biol* **315**:42–54. doi:10.1016/j.ydbio.2007.11.037

- Powell-Coffman JA, Knight J, Wood WB. 1996. Onset of *C. elegans* Gastrulation Is Blocked by Inhibition of Embryonic Transcription with an RNA Polymerase Antisense RNA. *Dev Biol* **178**:472–483. doi:10.1006/dbio.1996.0232
- Priess JR, Thomson JN. 1987. Cellular interactions in early *C. elegans* embryos. *Cell* **48**:241–250. doi:10.1016/0092-8674(87)90427-2
- R Core Team. 2014. R: A language and environment for statistical computing. R Foundation for Statistical Computing, Vienna, Austria.
- Raj A, Rifkin SA, Andersen E, van Oudenaarden A. 2010. Variability in gene expression underlies incomplete penetrance. *Nature* **463**:913–918. doi:10.1038/nature08781
- Richards JL, Zacharias AL, Walton T, Burdick JT, Murray JI. 2013. A quantitative model of normal *Caenorhabditis elegans* embryogenesis and its disruption after stress. *Dev Biol* **374**:12–23. doi:10.1016/j.ydbio.2012.11.034
- Rivers DM, Moreno S, Abraham M, Ahringer J. 2008. PAR proteins direct asymmetry of the cell cycle regulators Polo-like kinase and Cdc25. *J Cell Biol* **180**:877–885. doi:10.1083/jcb.200710018
- Rose L, Gönczy P. 2014. Polarity establishment, asymmetric division and segregation of fate determinants in early *C. elegans* embryos. *WormBook Online Rev C Elegans Biol* 1–43. doi:10.1895/wormbook.1.30.2
- Sadler PL, Shakes DC. 2000. Anucleate *Caenorhabditis elegans* sperm can crawl, fertilize oocytes and direct anterior-posterior polarization of the 1-cell embryo. *Dev Camb Engl* **127**:355–366.
- Sarov M, Murray JI, Schanze K, Pozniakovski A, Niu W, Angermann K, Hasse S, Rupprecht M, Vinis E, Tinney M, Preston E, Zinke A, Ernst S, Teichgraber T, Janette J, Reis K, Janosch S, Schloissnig S, Ejsmont RK, Slightam C, Xu X, Kim SK, Reinke V, Stewart AF, Snyder M, Waterston RH, Hyman AA. 2012. A Genome-Scale Resource for In Vivo Tag-Based Protein Function Exploration in *C. elegans*. *Cell* **150**:855–866. doi:10.1016/j.cell.2012.08.001
- Schauer IE, Wood WB. 1990. Early *C. elegans* embryos are transcriptionally active. *Dev Camb Engl* **110**:1303–1317.
- Schindelin J, Arganda-Carreras I, Frise E, Kaynig V, Longair M, Pietzsch T, Preibisch S, Rueden C, Saalfeld S, Schmid B, Tinevez J-Y, White DJ, Hartenstein V, Eliceiri K, Tomancak P, Cardona A. 2012. Fiji: an open-source platform for biological-image analysis. *Nat Methods* **9**:676–682. doi:10.1038/nmeth.2019
- Schlesinger A, Shelton CA, Maloof JN, Meneghini M, Bowerman B. 1999. Wnt pathway components orient a mitotic spindle in the early *Caenorhabditis elegans* embryo without requiring gene transcription in the responding cell. *Genes Dev* **13**:2028–2038.
- Schubert CM, Lin R, de Vries CJ, Plasterk RHA, Priess JR. 2000. MEX-5 and MEX-6 Function to Establish Soma/Germline Asymmetry in Early *C. elegans* Embryos. *Mol Cell* 671–682. doi:10.1016/S1097-2765(00)80246-4
- Schulze J, Schierenberg E. 2011. Evolution of embryonic development in nematodes. *EvoDevo* **2**:18. doi:10.1186/2041-9139-2-18
- Schulze J, Schierenberg E. 2009. Embryogenesis of *Romanomermis culicivorax*: An alternative way to construct a nematode. *Dev Biol* **334**:10–21. doi:10.1016/j.ydbio.2009.06.009
- Shelton CA, Bowerman B. 1996. Time-dependent responses to glp-1-mediated inductions in early *C. elegans* embryos. *Development* **122**:2043–2050.
- Shimizu T, Ishii R, Takahashi H. 1998. Unequal cleavage in the early *Tubifex* embryo. *Dev Growth Differ* **40**:257–266. doi:10.1046/j.1440-169x.1998.00001.x
- Srinivasan DG, Fisk RM, Xu H, Heuvel S van den. 2003. A complex of LIN-5 and GPR proteins regulates G protein signaling and spindle function in *C. elegans*. *Genes Dev* **17**:1225–1239. doi:10.1101/gad.1081203
- Stevens H, Williams AB, Michael WM. 2016. Cell-Type Specific Responses to DNA Replication Stress in Early *C. elegans* Embryos. *PLOS ONE* **11**:e0164601. doi:10.1371/journal.pone.0164601

- Sulston JE, Schierenberg E, White JG, Thomson JN. 1983. The embryonic cell lineage of the nematode *Caenorhabditis elegans*. *Dev Biol* **100**:64–119. doi:10.1016/0012-1606(83)90201-4
- Thorpe CJ, Schlesinger A, Carter JC, Bowerman B. 1997. Wnt Signaling Polarizes an Early *C. elegans* Blastomere to Distinguish Endoderm from Mesoderm. *Cell* **90**:695–705. doi:10.1016/S0092-8674(00)80530-9
- Tibshirani R. 1996. Regression Shrinkage and Selection via the Lasso. *J R Stat Soc Ser B Methodol* **58**:267–288.
- Tinevez J-Y, Perry N, Schindelin J, Hoopes GM, Reynolds GD, Laplantine E, Bednarek SY, Shorte SL, Eliceiri KW. 2017. TrackMate: An open and extensible platform for single-particle tracking. *Methods San Diego Calif* **115**:80–90. doi:10.1016/j.ymeth.2016.09.016
- Tsou M-FB, Ku W, Hayashi A, Rose LS. 2003. PAR-dependent and geometry-dependent mechanisms of spindle positioning. *J Cell Biol* **160**:845–855. doi:10.1083/jcb.200209079
- Valfort A-C, Launay C, Sémon M, Delattre M. 2018. Evolution of mitotic spindle behavior during the first asymmetric embryonic division of nematodes. *PLOS Biol* **16**:e2005099. doi:10.1371/journal.pbio.2005099
- Yamamoto K, Kimura A. 2017. An asymmetric attraction model for the diversity and robustness of cell arrangement in nematodes. *Development* **144**:4437–4449. doi:10.1242/dev.154609
- Zacharias AL, Murray JI. 2016. Combinatorial decoding of the invariant *C. elegans* embryonic lineage in space and time. *genesis* **54**:182–197. doi:10.1002/dvg.22928

Figure legends

Figure 1 – Two methods for equalizing first cell division in *C. elegans* embryos

(A) The ternary complex comprised of G α , GPR-1/2 and LIN-5 dimers tethers a dynein complex (only the motor protein is represented here) to the cell cortex, thereby generating pulling forces on astral microtubules (top). The *lin-5(ev571)* temperature-sensitive mutant encodes a protein with a 3-amino acid insertion (red disc) in the coiled-coil domain; this mutant protein cannot dimerize or generate pulling forces at the restrictive temperature (bottom).

(B) Scheme of transient temperature upshift during the first division of the *C. elegans* zygote to equalize AB and P₁ sizes using *lin-5(ev571)*. Such transient upshift has no impact on the asymmetry of the first unequal division in the wild type, yielding AB and P₁ cells corresponding to ~60% and 40% of embryo size, respectively (middle), due to asymmetric net cortical pulling forces acting on the spindle poles (arrows), stemming from the posterior enrichment of the ternary complex (orange). Cortical pulling forces are impaired upon transient upshift of *lin-5(ev571)* embryos, resulting in equalized first division (bottom). The red dashed line indicates the embryo center. Embryos are oriented with anterior to the left here and all figure panels.

(C) DIC images from time-lapse recordings at the 2-cell stage (left) and 20 hours thereafter (right). Upshifted wild-type embryo (top) or *lin-5(ev571)* embryo kept at 17°C (middle) divide unequally and develop into 3-fold larvae that later hatch, while upshifting *lin-5(ev571)* embryos results in equalized division (bottom), which can result in embryonic lethality. In this and other figure panels, scale bar is 10 μ m and relative AB cell size at 2-cell is indicated. See also Videos 1-3.

(D) Scheme of optogenetic-mediated LIN-5::ePDZ::mCherry recruitment to the anterior cortex by localized activation of PH::eGFP::LOV interaction with a 488 nm laser light. A helix in the LOV domain unfolds upon illumination, allowing binding of ePDZ. Stars represent fluorescent protein fusion (GFP: grey to start with, green upon illumination; mCherry: red).

(E) Embryos expressing LIN-5::ePDZ::mCherry and PH::eGFP::LOV divide unequally without 488 nm light exposure, due to asymmetric localization of LIN-5 (top). Optogenetic-mediated recruitment of LIN-5::ePDZ::mCherry to the anterior cortex during mitosis (blue rectangle) results in balanced net pulling forces on the two spindle poles and equal first division (bottom).

(F) Images from time-lapse recording of optogenetic-mediated first division equalization. LIN-5::ePDZ::mCherry was recruited to the anterior cortex from anaphase onset until cytokinesis completion by scanning the 488 nm laser in the indicated rectangular region. Note that endogenous LIN-5 is tagged with ePDZ::mCherry, hence resulting in the fusion protein being present also on the spindle, the centrosomes and the posterior cortex during anaphase.

1101 Note that that this strain also expresses GFP::TBB-2, which is not visible in the small
1102 illuminated portion of the cortex. Time indicated in min:s. See also Video 4.

1103 **Figure 1 – supplement 1 - Cell size measurement method and precision**

1104 **(A)** The surfaces of AB and P₁ were determined in the mid-plane image with the largest cross-
1105 sectional area. Cell boundaries were manually traced using the GFP::PH signal labeling the
1106 plasma membrane with the polygon tool in Fiji and the enclosed surface measured. Scale bar
1107 is 10 µm in this and all Supplemental figure panels (left).

1108 **(B)** Mean variation coefficient of repeated manual measurements of AB cell surface in 25
1109 embryos, corresponding to the technical error, which is 0.66% ± 0.27 SD on average; each
1110 embryo was independently measured 3-5 times (right).

1111 **(C)** Cell volumes were segmented automatically using the Interactive Morphological 3D
1112 reconstruction plugin in Fiji, and the relative AB volume with respect to the sum of AB and P₁
1113 volumes calculated.

1114 **(D)** Correlation of relative AB surface and AB volume. Solid black line: linear model fitted to
1115 the data; grey dashed lines: 95% confidence interval for the fit.

1116 **(E)** Mean percentage error of relative AB size based on the difference between surface and
1117 volume measurements as a function of relative AB size, showing that there is no significant
1118 correlation between the two. Same embryos as in panel C.

1119 See also Figure 1 – supplement 1 – source data and Figure 1 – supplement 1 – source code

1120 **Figure 1 – supplement 2 – Upshifted *lin-5(ev571)* embryos are polarized**

1121 **(A, B)** Distribution (A) and corresponding quantification of normalized cytoplasmic intensity (B)
1122 of endogenously tagged PAR-2::GFP in control (Ctrl) and upshifted *lin-5(ev571)* embryos
1123 (Up). Note that in this case the control *lin-5(ev571)* condition included 13 non-upshifted
1124 embryos and 5 embryos upshifted in the early 2-cell stage (denoted with *).

1125 **(C, D)** Distribution (C) and corresponding quantification of normalized cytoplasmic intensity
1126 (D) of endogenously tagged mCherry::MEX-5 in control (Ctrl) and upshifted *lin-5(ev571)*
1127 embryos (Up).

1128 See also Figure 1 – supplement 2 – source data and Figure 1 – supplement 2 – source code

1129

1130 **Figure 1 – supplement 3 – Ventral rupture in equalized embryos**

1131 **(A)** Four time-points from DIC recording of hypodermal ventral closure in control *lin-5(ev571)*
1132 embryo upshifted at the 2-cell stage. Hypodermal cells migrate from both sides towards the
1133 ventral midline (yellow arrows indicate movement), where they meet and seal the embryo in a
1134 continuous skin layer. The embryo flips on its side at the comma stage when the elongation

phase of morphogenesis begins. In this and other Supplemental figure panels, relative AB cell size at 2-cell is indicated. See also Video 5.

(B) Incomplete ventral closure (red dashed area) in upshifted *lin-5(ev571)* embryo that will later die, with extrusion of internal tissues (red arrows). The resulting phenotype at 06:10 shows pharyngeal (white dashed area) and gut (red dashed area) tissue partially squeezed outside of the body cavity. Time is indicated in min:s, with time 0 corresponding to ~6 hours after first cleavage at 17°C, when the first lateral movements of ectoderm towards the midline begin and become visible as a slight lateral contraction of the embryo. See also Video 6.

(C) Postembryonic phenotypes in control and upshifted *lin-5(ev571)* animals recovered as embryos shortly after the upshift (Materials and Methods). pv – protruding vulva, ste – sterile, egl – egg laying defective. See source data for detailed breakdown of phenotypes in individual embryos. See also Figure 1 - supplement 3 - source data for detailed breakdown of phenotypes in individual embryos.

Figure 2 – Equalized first cell division decreases embryonic viability

(A) Box plots of relative AB size distribution determined in the mid-plane (here and thereafter) in embryos of the indicated conditions; Upshifted (Up) wild-type (Wt), *lin-5(ev571)* kept at 17°C (No Up), *lin-5(ev571)* upshifted in the early 2-cell stage (Control), as well as *lin-5(ev571)* upshifted during the first mitotic division and binned into embryos that later lived (Alive) or died (Dead). Here and in other figure panels, two boxplots that do not share the same letter are significantly different from each other with $p < 0.05$; Welch t-test. See Supplementary File 6 for exact p value and complete statistical analyses for this and all other figures. Dashed line here and in (C) indicate equal AB and P₁ sizes.

(B) Lethality of embryos of from (A), with Alive and Dead categories binned as a function of relative AB size and an indication of the number of embryos in each bin. Brackets indicate a mathematical notation for the size interval, with an inclusion of the value next to the square bracket], but not of that next to the round bracket), so that individual bins do not overlap.

(C) Relative AB size in embryos expressing LIN-5::ePDZ::mCherry and PH::eGFP::LOV, either not subjected to 488 nm laser light (left, n=13) or equalized through optogenetic recruitment of LIN-5 to the anterior cortex (right, n=56).

(D) Lethality of embryos from (C) as a function of relative AB size; binning as in (B). “Plates” refers to embryos expressing LIN-5::ePDZ::mCherry and PH::eGFP::LOV scored for hatching on plates, without filming.

(E) Division asynchrony between AB and P₁ as a function of AB size in upshifted *lin-5(ev571)* embryos; time was determined using anaphase onset monitored with mCherry::H2B. Shown is the subset of *lin-5(ev571)* control and upshifted embryos from (A) for which AB-P₁ asynchrony was measured. Pearson’s correlation value (r) is shown here and in subsequent figure panels,

together with significance of association between two variables determined via the asymptotic t approximation (cor.test function in R, p).

(F) Division asynchrony between AB and P₁ in embryos of indicated conditions; upshifted *lin-5(ev571)* embryos were split into two bins as a function of AB sizes, as shown. Percentage above each boxplot indicates proportion of embryonic lethality; blue: illumination of P₁ with 405 nm laser to delay cell cycle progression and restore asynchrony between AB and P₁. Non-illuminated embryos: same data as in (E). Dashed line indicates mean time difference in control embryos.

See also Figure 2 – source data and Figure 2 – source code for underlying analysis and data for this figure.

Figure 2 – supplement 1 – Aberrant blastomere arrangement at the 4-cell stage

(A, C) Maximal Z-projection from fluorescent timelapse recording of *lin-5(ev571)* embryos expressing GFP::PH and mCherry::H2B to mark the plasma membrane and chromatin, respectively. In the wild type, as well as in control *lin-5(ev571)* embryos kept at 17°C (shown here), AB divides before P₁ resulting in a characteristic 4-cell rhomboid arrangement. Time is indicated in min:s since the beginning of the recording.

(B) Normally, P₂ is in contact with ABp and EMS, so that Delta signaling from P₂ induces proper fate acquisition of ABp, distinguishing it from ABa, whereas Wnt/Src signaling from P₂ induces polarization of EMS.

(C) A minor fraction of upshifted *lin-5(ev571)* embryos fail to sufficiently skew the AB cell during division, leading to a T-arrangement at the 4-cell stage, whereby P₂ does not contact any of the two AB daughter cells, presumably preventing Delta signaling. See also Video 7.

(D) Schematic of abnormal T-arrangement at the 4-cell stage in a minor fraction of upshifted *lin-5(ev571)* embryos, which prevents instructive signaling between P₂ and ABp.

Note that upshifted *lin-5(ev571)* embryos with a T-arrangement were more elongated than those with a normal rhomboid arrangement (59.6 ± 2.83 and 55.0 ± 2.75 μ m, $p < 0.0003$ for Welch's two-sample t test, $n = 10$ and 80 measured for this trait, respectively). However, the eggshell length of *lin-5(ev571)* embryos is not different from that of wild-type embryos (54.4 ± 2.8 μ m and 55μ m ± 1.7 , respectively, $p = 0.39$, $n=10$ and 80).

Figure 3 - Faster cell cycle progression in P₁ descendants of equalized embryos results in altered division sequence.

(A, B) Number of cells in the AB (A) and P₁ (B) lineages starting from the 4-cell stage in embryos of indicated conditions. Dashed rectangular region is enlarged on the right. In this

and subsequent figure panels, time 0 corresponds to ABa cleavage. Dotted lines -most visible in the enlargements on the right- indicate standard deviations.

(C) Graphical depiction of differences in cell cycle timing in individual cells of the AB (top) and P₁ (bottom) lineages at the 26-cell stage; colors indicate relative change of cell cycle timing in equalized *lin-5(ev571)* embryos compared to control *lin-5(ev571)* condition. In each panel, empty circles represent cells of the other lineage.

(D) Partial lineage tree of a control *lin-5(ev571)* embryo (top) and an equalized *lin-5(ev571)* embryo (bottom). Normally, P₄ divides only once to produce the germline precursors Z2 and Z3, which remain quiescent until hatching (top). In some equalized and inverted embryos, P₄ divides more than once, suggesting a repetition of the P₃ fate or a fate transformation towards a D-like state (bottom, labeled by question mark). Also, a global acceleration of the C and D lineages is apparent in the equalized embryo compared to the control. Vertical grid lines and time indicated on the x axis correspond to division of P₂, P₃, D, and P₄ in the control embryo.

(E) Frequency of embryos with one or more extra divisions in the P₄ lineage in indicated conditions (dark grey), with number of analyzed embryos shown on top. Light grey corresponds to embryos with a normal phenotype here and in similar panels in other figures. Lethality is not significantly more frequent in dying embryos (Fisher's exact test, p=0.33).

(F) Temporal division sequence in embryos in indicated conditions. Note that the faster cell cycle of P₁ lineage cells in equalized and inverted embryos leads to an altered division sequence, highlighted by connecting red lines and arrows for Ea, D, P₄ and Da. Dark horizontal bars indicate standard error of the mean. Not all AB cells are shown due to space constraints, but the first and last AB cell in each division round are indicated.

(G) Variability in cell cycle duration in AB and P₁ lineage expressed as variation coefficient to normalize for cell cycle duration in different cells. Color code as in panel A. Here and in Fig. 4C-D, letters above groups indicate statistical comparison of overall variability among five groups using Anova and Tuckey honest significant difference (HSD) post-hoc test for all pairwise combinations, whereas comparisons between AB and P₁ lineages within groups are indicated below boxplots using Welch's two sample t-test; asterisks indicate significance levels at 0.05 (*) or 0.001 (**).

Figure 3 – supplement 1 – Correlation of cell cycle with AB size in *lin-5(ev571)* embryos

Cell cycle duration correlates with initial size asymmetry in most P₁ lineage cells (orange), but rarely in AB lineage cells (blue). Note that this analysis included all upshifted and control *lin-5(ev571)* embryos to obtain most reliable correlation of cell-cycle duration with initial size-asymmetry. Vertical lines indicate 95% confidence interval for correlation coefficient value. Cells with significant Pearson correlation are indicated by filled discs ($p < 0.05$, corrected for multiple testing with the Benjamini-Hochberg method), whereas empty circles indicate differences that are not statistically significant. Detailed results of statistical tests for each cell are in Supplementary File 3.

Figure 4 – Cell division axis and cell position are frequently altered in equalized embryos

(A, B) Mean positional deviation (A) or angular deviation (B) \pm SD per cell over time in embryos of indicated conditions compared to control *lin-5(ev571)* reference. The mean positional deviation per cell was calculated at 1-minute intervals as the sum of Euclidian distances of individual cells divided by the number of cells at that stage. Only embryos lineaged past the 15-cell stage were included in this analysis.

(C, D) Variability in cell position deviation (C) and angular deviation of division orientation (D) in embryos of indicated conditions expressed as SD for cells between 25-180 minutes of development (time 0 corresponds to ABa division).

(E) Compression (sample height) in embryos of indicated conditions. Comparisons between groups were performed using an HSD post-hoc test.

(F) Angular deviation of EMS spindle at anaphase onset in embryos of indicated conditions compared to the control *lin-5(ev571)* reference. Note that the four live equalized embryos exhibiting a $>35^\circ$ EMS skew at anaphase onset corrected spindle orientation to near normality during late anaphase.

(G) Nuclear positions in the control *lin-5(ev571)* reference shown with black spheres, connected by lines with the position of the corresponding nuclei in an equalized *lin-5(ev571)* embryo exhibiting the EMS skew; sphere size is proportional to nuclear diameter. The skew in EMS division leads to mispositioning of E and MS at the 8-cell stage (highlighted by red line; top), resulting in widespread positioning defects at the 15-cell stage (bottom) and thereafter (not shown). Here and in (J), dashed line indicates center of the L-R axis. The directions of the three embryonic axes are depicted here and in other panels.

(H) Deviation of MS division orientation angle in embryos of indicated conditions compared to the control *lin-5(ev571)* reference.

(I) Mispositioning of MSa and MSp in equalized *lin-5(ev571)* embryos measured as a distance to corresponding positions in the control *lin-5(ev571)* reference.

(J) Positions of nuclei in equalized *lin-5(ev571)* embryo with L-R inversion of MSa and MSp (MSa and MSp: magenta, Ea and Ep: yellow), connected by lines to cell positions in the control *lin-5(ev571)* reference, indicated as small black spheres.

(K) Quantification of MSa/MSp inversion phenotype in indicated conditions scored prior to MSa/MSp division; the phenotype is significantly associated with the outcome of development among equalized *lin-5(ev571)* embryos (Fisher's exact test, $p=0.007$).

Figure 4 – supplement 1 - Systematic analysis of features in lineaged embryos up to 15-cell stage

(A) Volcano plot illustrating selection of significant features (red and purple, with purple indicating MS related features) comparing equalized dead and equalized alive *lin-5(ev571)* embryos up to the 15-cell stage (p -value < 0.008 , corresponding to a $<10\%$ false discovery rate and a change of at least $\pm 15\%$ between groups, indicated by dashed lines). Features are encoded as a combination of cell name and measured value in the following way: netdis -net total displacement of given cell during its lifetime; aXX and pXX –division angle and positional deviation, respectively, with XX referring to the direction, i.e. AP = antero-posterior, DV = dorso-ventral, LR = left-right; overall angular (aMean) or spatial (pOV) deviation. Note that embryos with skewed EMS division were excluded from this analysis due to their substantial defects. See Supplementary File 4 for details.

(B) Correlogram of significant features from (A). Significant pairwise Pearson correlations are indicated with overlaid white asterisks (p -value $* < .05$, $** < .001$, $*** < .001$, association test based on the t statistics for two normally distributed variables). Embryo size and compression (sample height) were added to explore possible effects of physical factors on the selected features.

Figure 5 – Incomplete fate acquisition in endodermal and pharyngeal lineages in equalized *lin-5(ev571)* embryos

(A) Gastrulation in *C. elegans* begins with ingression of Ea/Ep. Actual embryo viewed by DIC with partial overlay (top), and enlarged corresponding schematic (bottom).

(B) Gastrulation is accompanied by a nearly 2-fold lengthening of the Ea/Ep cell cycle compared to that of their MSa/MSp cousins. Ea/Ep normally divide after internalization. Red arrow indicates usual delay between MSp and Ea/Ep divisions shown in panel C.

(C) Time delay between MSp and Ea/Ep divisions in embryos of indicated conditions.

(D) Average trajectory of Ea/Ep interphase nucleus as a function of initial AB size. Here and in (F): same color code as in (C); moreover, marginal boxplots show overall distribution of

individual groups of corresponding color, with letters indicating whether the mean differs statistically between groups (Welch t-test, $p < 0.05$).

(E) END-3::GFP expression in Ea/Ep (dashed area) in control and equalized *lin-5(ev571)* embryo; Ea/Ep cells in the latter divide close to the eggshell, before completing ingress. Higher magnification views on the right show the time point with peak END-3::GFP expression. Time is indicated in h:min from the time of first cleavage. See also Video 8.

(F) Quantification of END-3::GFP peak expression during the Ea/Ep cell cycle as a function of initial AB size. Statistical comparisons are indicated using the letters code above the marginal boxplot (Welch's test, BH corrected p -value < 0.05)

See also Figure 5 - source data and Figure 5 - source code for analysis for panels C-F

(G) Control (top) or equalized dead *lin-5(ev571)* (bottom) ~100-cell stage embryo expressing GFP::PH (not shown) and ELT-2::GFP in inverted black and white rendition. Note that the image of the control embryo has been rotated, explaining the white areas in the corners.

(H) Quantification of embryos with abnormal ELT-2::GFP expression (defined as < 8 GFP positive cells at the ~100-cell stage) in indicated conditions. Lethality of equalized embryos is not significantly associated with ELT-2::GFP expression pattern ($p = 0.69$, Fisher's exact test)

(I) Expression of PHA-4::GFP in inverted black and white rendition at the ~100 cell stage in an equalized alive (top) and an equalized dead (bottom) *lin-5(ev571)* embryo.

(J) Quantification of embryos with abnormal PHA-4::GFP expression at the ~100 cell stage in indicated conditions. Lethality of equalized embryos is not significantly associated with PHA-4::GFP expression pattern ($p = 0.128$, Fisher's exact test). See Fig. 5 – supplement E for detailed annotation of expression patterns.

Figure 5 – supplement 1 – Fate acquisition in endodermal and pharyngeal lineages

(A) Trajectory of Ea and Ep nuclei in embryos of indicated conditions compared with Welch two sample t test; * $< .05$, ** $< .001$.

(B) Correlation between average trajectory and cell cycle duration in Ea/Ep. Same color code as in (A) here and in (C).

(C) Correlation between average END-3::GFP expression levels and average cell cycle duration in Ea/Ep. See also Figure 5 – source data and Figure 5 – source code for underlying data and analysis for panels A-C

(D) Scheme of anterior pharynx induction in ABalp and ABara descendants via Delta/Notch signaling emanating from MS/MSa/MSP. The GLP-1 Notch receptor (thick black lines) is expressed on the surface of all ABa cells, but ABala and ABarp normally have no physical contact with the signaling MS cells, such that they are not induced.

(E) PHA-4::GFP distribution assessed by scoring the identity of GFP positive cells at the ~100-cell stage in equalized *lin-5(ev571)* embryos. X in the cell designations (e.g. MSpaaXX) stands for a/p; therefore, XX comprises four cells: aa, ap, pa, pp. Asterisks indicate two inverted embryos with aberrant pattern that were included in this analysis.

Figure 6 – logistic Lasso regression machine learning analysis predicts lethality in early equalized embryos

(A) Prediction accuracy of lethality versus survival in equalized embryos for individual logistic Lasso models generated by 5-fold cross-validation (CV) over 250 repetitions in indicated stages. Note that embryos with a T-arrangement at the 4-cell stage or with a skewed EMS division at the 6-cell stage were excluded from this analysis, as were embryos with missing values for some of the cells.

(B) Number of predictive features in individual Lasso models over CV 250 iteration; 14 alive and 17 dead equalized *lin-5(ev571)* embryos were used for training. Y-axis: number of iterations in which a model with the indicated number of features was selected. Zero features dominant at the 4-cell stage indicates that an empty model (intercept only) was selected in the majority of iterations and performed poorly overall.

(C) Inclusion frequency of individual features in an optimal model at each CV iteration over 250 repetitions at indicated stages. Selected variables were chosen from 18, 72, 150 and 249 features present at 4-, 8-, 15- and 28-cell stage, respectively. Supplementary File 7 lists all features used at each stage used for Lasso analysis.

(D) Receiver operator curve (ROC) of best model selected at each stage with the minimal cross-validation error. Shown are selectivity and sensitivity as a function of changing the threshold value for assigning embryos to dead or alive category; diagonal line: random classification. We noted also that even though the models at the 8-cell stage had inferior accuracy, MS division orientation was repeatedly selected among four predictive features at that stage, highlighting the importance of the MSa and MSp inversion phenotype described in Figure 4.

Figure 6 – supplement 1 – Summary of phenotypes observed in equalized and inverted *lin-5(ev571)* embryos.

(A, B) Fraction of equalized (alive or dead, as indicated) and inverted *lin-5(ev571)* embryos displaying a given phenotype (A), or not (B), with number of embryos analyzed for each trait indicated above the bars. Unequal control *lin-5(ev571)* embryos showed no or minimal occurrence of these phenotypes; refer to previous figures for control scoring.

Figure 6 – supplement 2 - Comparison of cell positions at the 8- and 16-cell stage in equalized embryos

(A, B) Shown are dorsal (XY, top) and lateral (XZ, bottom) views at the 8- (A) and 16- cell stage (B). Ellipses indicate 50% confidence interval for nuclear position distributions among alive (grey) and dead (colored) *lin-5(ev571)* embryos. Arrows show direction of change between mean cell positions of the two groups. Bold arrows indicate significant difference in at least one direction (see Supplementary File 2 for statistics).

Figure 6 – supplement 3 – Comparison of variance and mean changes between equalized and control *lin-5(ev571)* embryos.

(A) Contingency table cross-tabulating features scored in the lineaging dataset with a significant change in mean and/or variance among equalized embryos compared to *lin-5(ev571)* control embryos. Welch's t-test and F-test with Benjamini-Hochberg correction were used.

(B-C) Number of significant features from (A) according to cell lineage and feature type (colored according to the legend), with significant change of mean or variance among equalized embryos.

(D) 23 features exhibit an increase in variance without a change in the mean. Note that there is not a single variable with increased variance among controls. See the source data for this figure for all 1608 features, p-values and the degree of change.

Supplementary videos

Video 1 - Unequal division of the wild type *C. elegans* zygote. The resulting 2-cell stage of this particular embryo had an AB size of 62% of the total embryo in the mid-plane. Note vertical rocking of spindle as it moves towards the posterior pole during anaphase. Time is indicated in min:s in this and all other videos. Embryos are ~50 um long.

Video 2- Unequal division of the *lin-5(ev571)* mutant zygote at the permissive temperature of 17°C (relative AB size 58%). Note severely dampened anaphase spindle rocking indicating reduced cortical pulling forces.

Video 3 - Transient upshift of *lin-5(ev571)* embryo from 17°C to 27°C from metaphase until the completion of cytokinesis results in equalized or even inverted division, as in this particular embryo, in which AB is smaller than P₁ (AB size 47%). Note severely dampened anaphase spindle rocking, indicating reduced cortical pulling forces.

Video 4 - Optogenetic recruitment of transgenic LIN-5 to the anterior cortex during mitosis counteracts posterior forces and results in equalized division (relative AB size 49%). Montage showing DIC recording (left), LIN-5::EPDZ::mCherry (middle) and PH::EGFP::LOV (right). LIN-5::EPDZ::mCherry was recruited to membrane-bound PH::EGFP::LOV by exposing a small rectangular region at the anterior cortex with a 488 nm laser during mitosis.

Video 5 - Ventral closure of epidermis at the end gastrulation in control *lin-5(ev571)* embryo at the permissive temperature of 17°C. Lateral cells migrate over ventral neuroblasts to enclose the embryo in a continuous epidermal layer called the hypodermis. Subsequently, differentiating muscles start to contract and the embryo gradually elongates into a tubular body shape. Time is indicated in h:min.

Video 6 – Upshifted equalized *lin-5(ev571)* embryo failing to undergo ventral epidermis closure, resulting in the extrusion of internal tissues from the body cavity as muscles start contracting. Embryo shown here had a relative AB size of 53%.

Video 7 - Equalized size of AB and P₁ leads to an aberrant T-arrangement at the 4-cell stage in ~4% of equalized embryos (relative AB size 50% in this case).

Video 8 - Expression of the endodermal marker END-3::GFP in control (left) and equalized (right) *lin-5(ev571)* embryos (relative AB size 58% and 53%, respectively). In the equalized embryo, Ea/Ep express less END-3::GFP than they normally do, and divide prematurely, before completing ingression.

Supplementary tables

Supplementary File 1 – Annotation of all lineaged embryos reported in this study in Figures 3 and 4

Supplementary File 2 – Statistical comparisons of all features (cell cycle timing, cell positions, division angles, migration) for individual cells between pairs of embryo groups (wild-type, controls, equalized alive, equalized dead, inverted)

Supplementary File 3 – Analysis of correlation between relative AB size and cell cycle duration in all *lin-5(ev571)* embryos from Supplementary File 1.

Supplementary File 4 – List of features between 4-15 cell stage and comparison of mean values between equalized alive and equalized dead *lin-5 (ev571)* embryos for the Volcano plot in Figure 4 – supplement 1A.

Supplementary File 5 – List of *C. elegans* strains used in this study.

1448 **Supplementary File 6** – Statistical comparisons, average values, and number of observations
1449 for the figures in this study, with the exception of lineaged embryos (Figures 3 and 4), for
1450 which values are provided in other supplementary files.

1451 **Supplementary File 7** – List of features used for Lasso analysis at 4-, 8-, 15-, and 28-cell
1452 stage, including inclusion frequency and model coefficients for best predictive models.

Figure 1

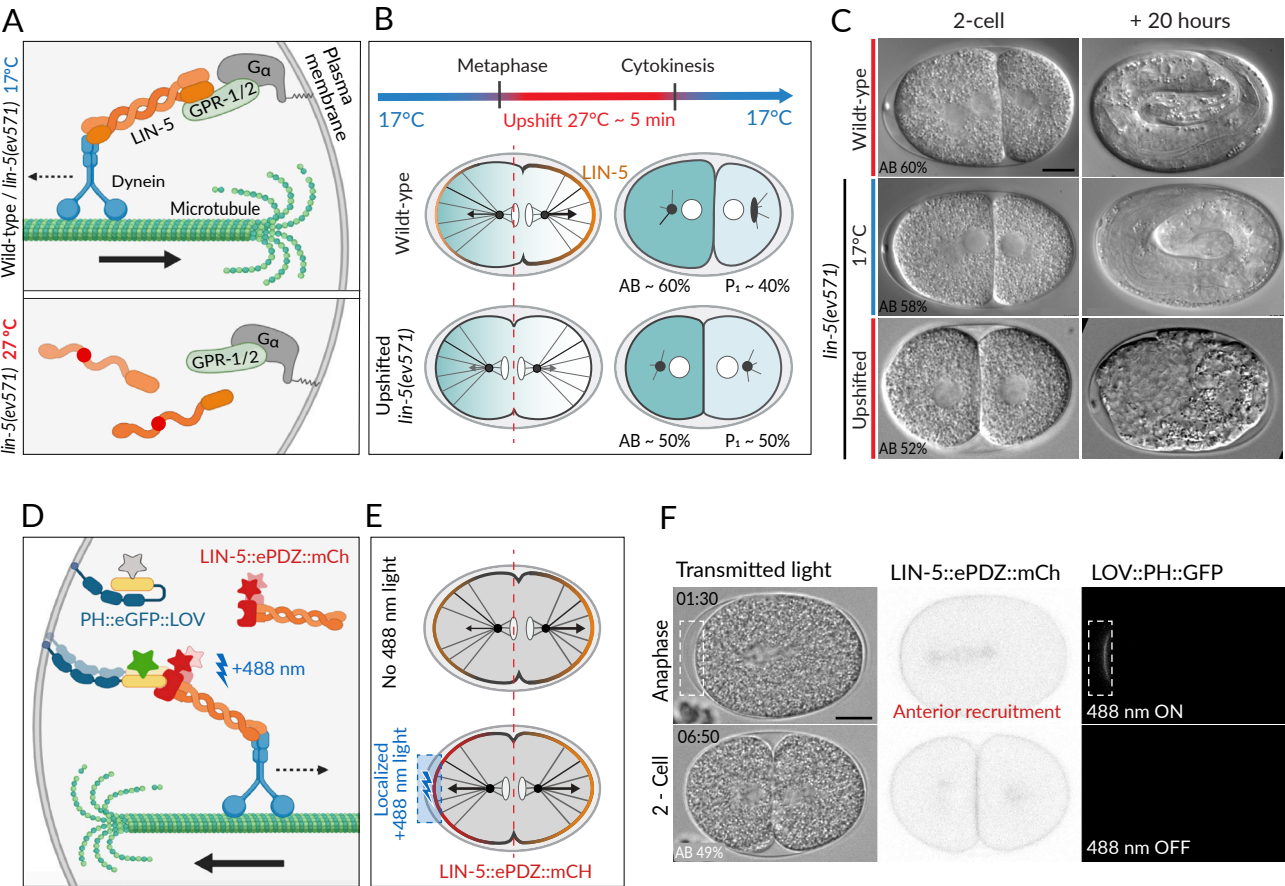


Figure 1 - supplement 1

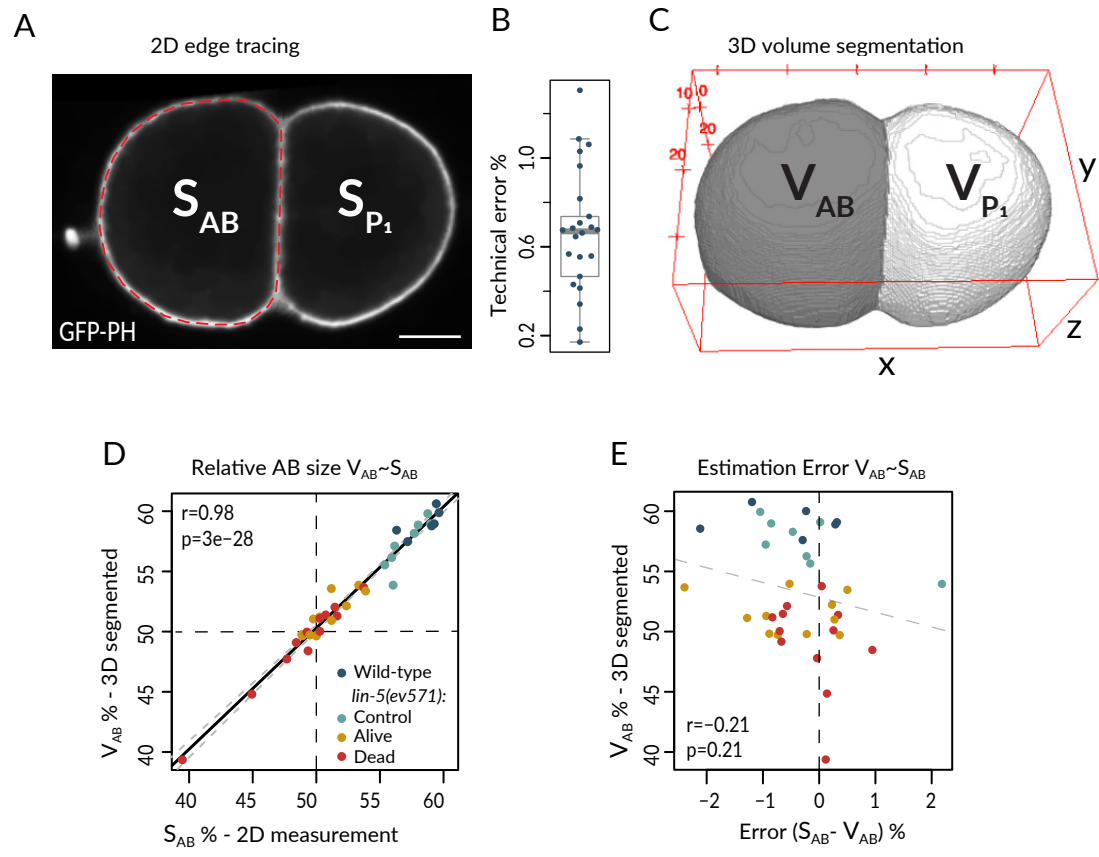


Figure 1 - supplement 2

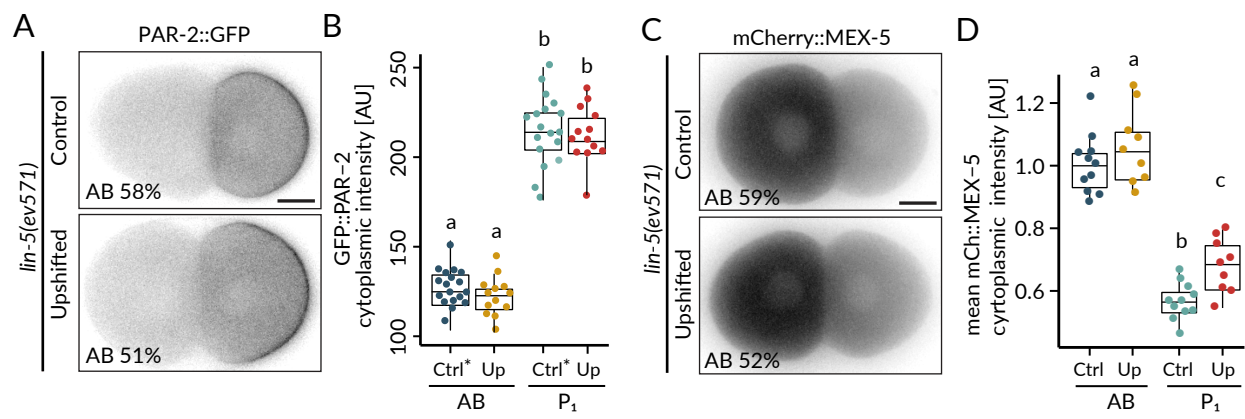
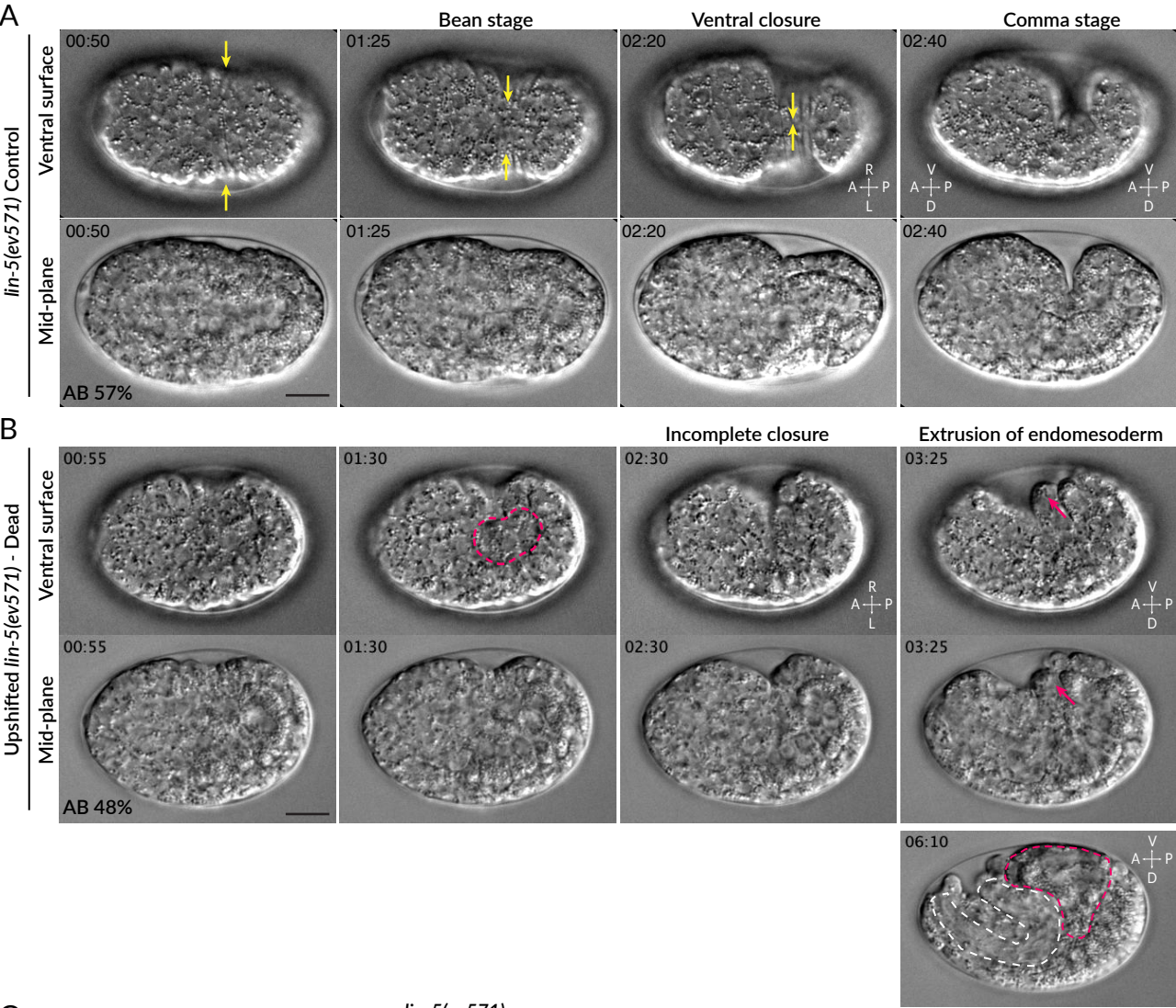


Figure 1 - supplement 3



C

lin-5(ev571)

	Controls			Equalized			Fisher test p-value	
	+	N	%	+	N	%		
Dead as L1/L2	2	20	10%	6	22	27%	0.243	n.s.
Visible adult phenotypes *	3	18	17%	9	16	56%	0.030	*
Reduced fertility **	1	18	6%	8	16	50%	0.006	*

* egl / ste / pv / gonad missing / less than 100 progeny

** less than 50 progeny

Figure 2

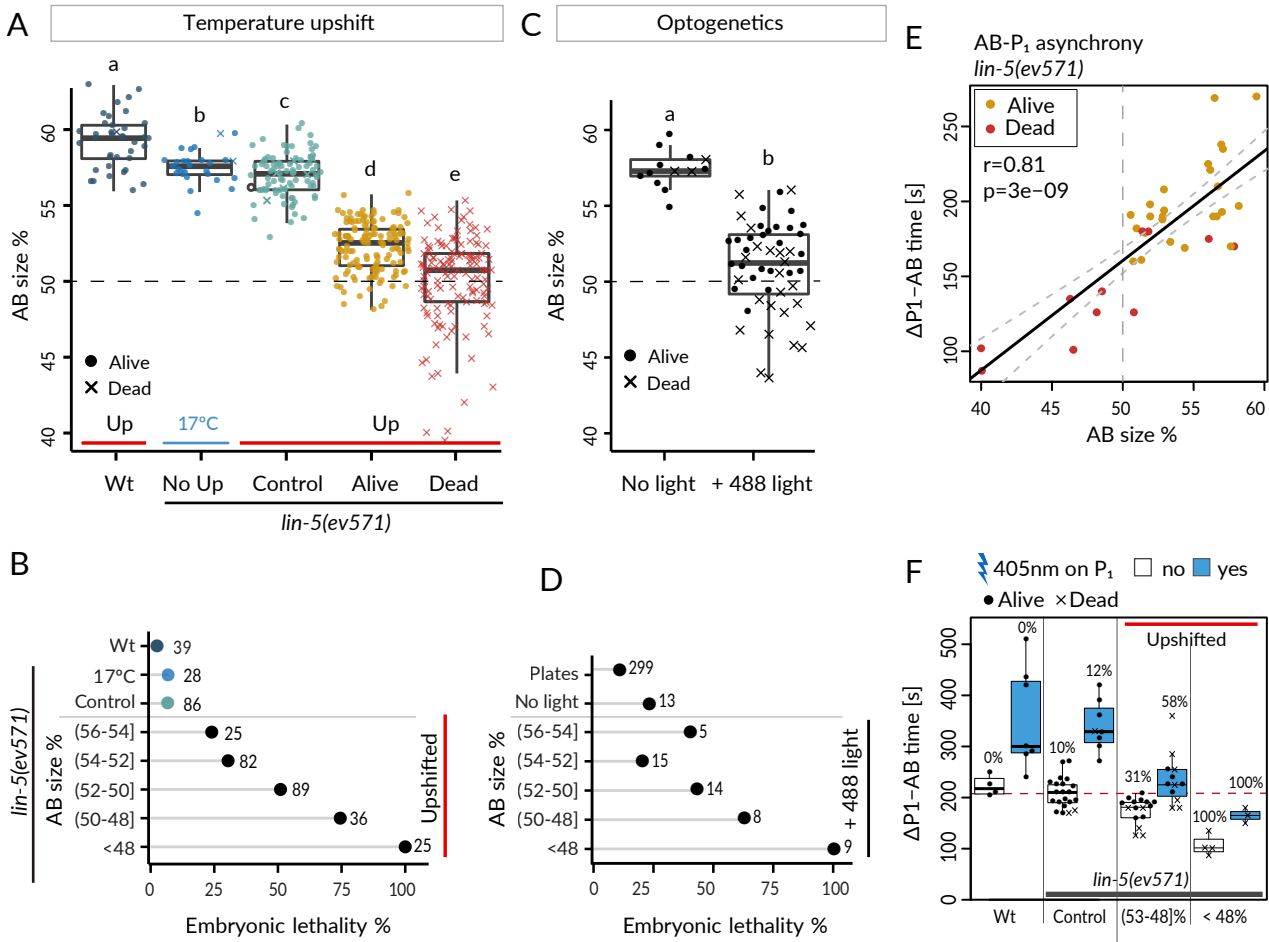


Figure 2 - supplement 1

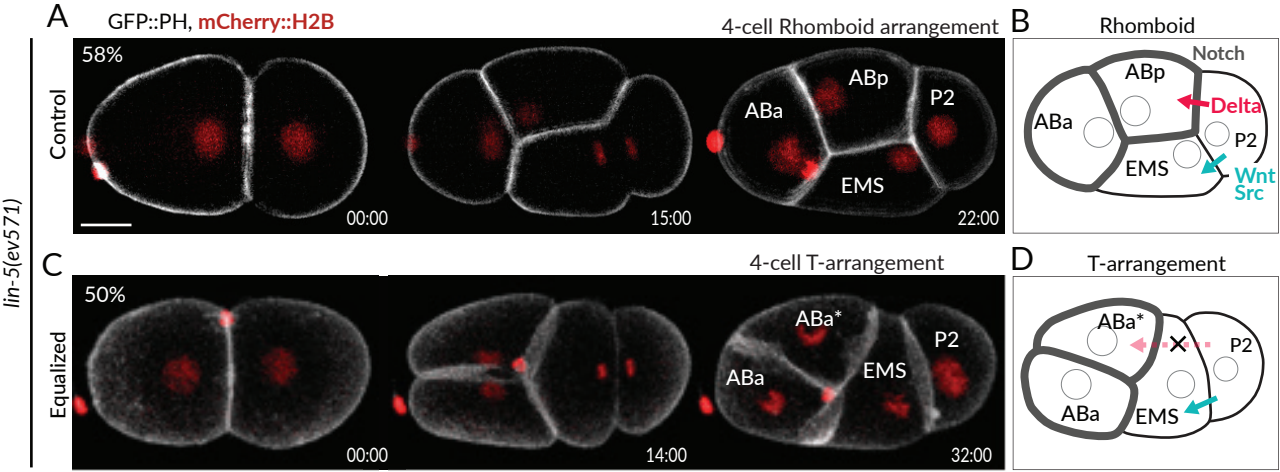


Figure 3

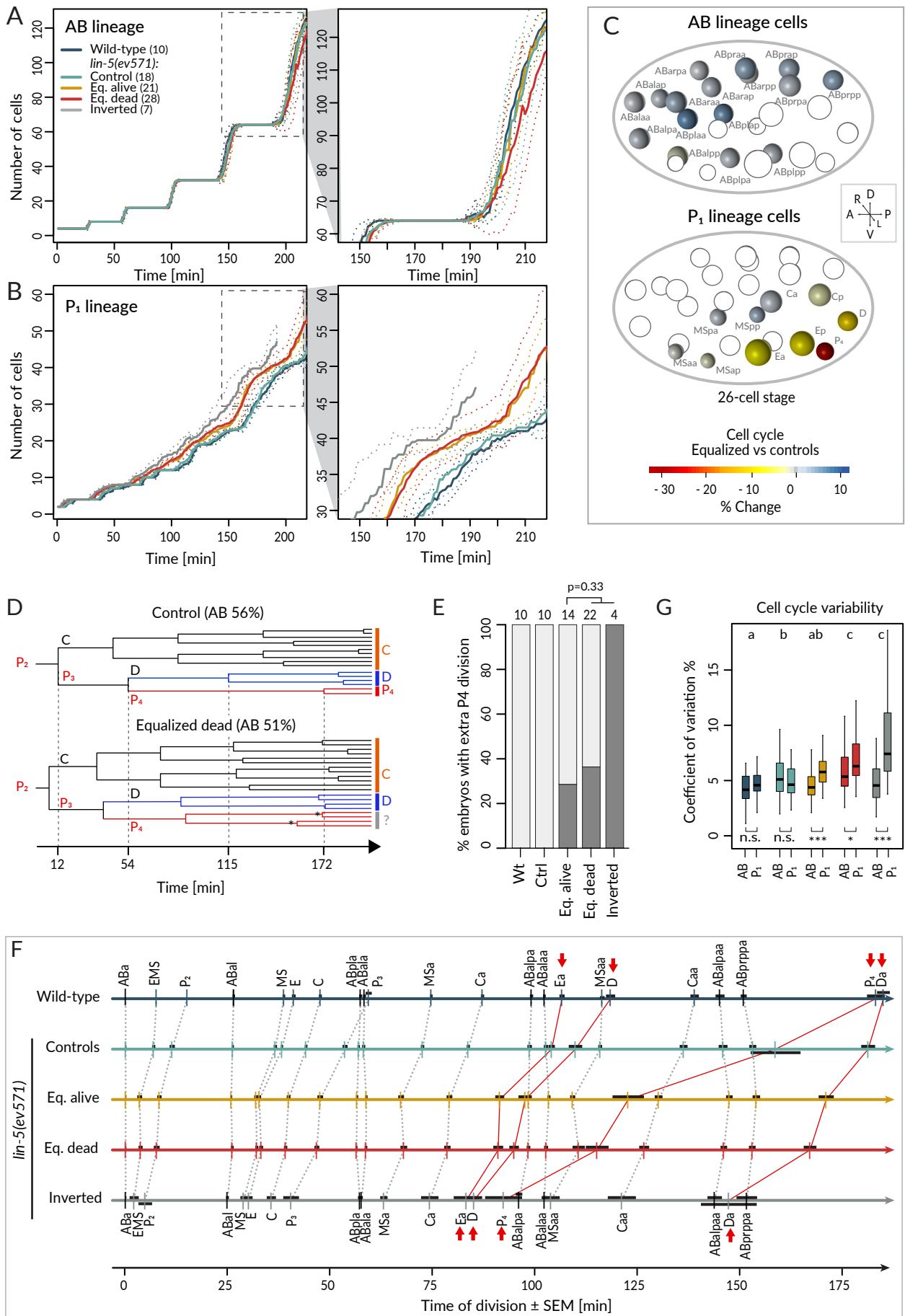


Figure 3 - supplement 1

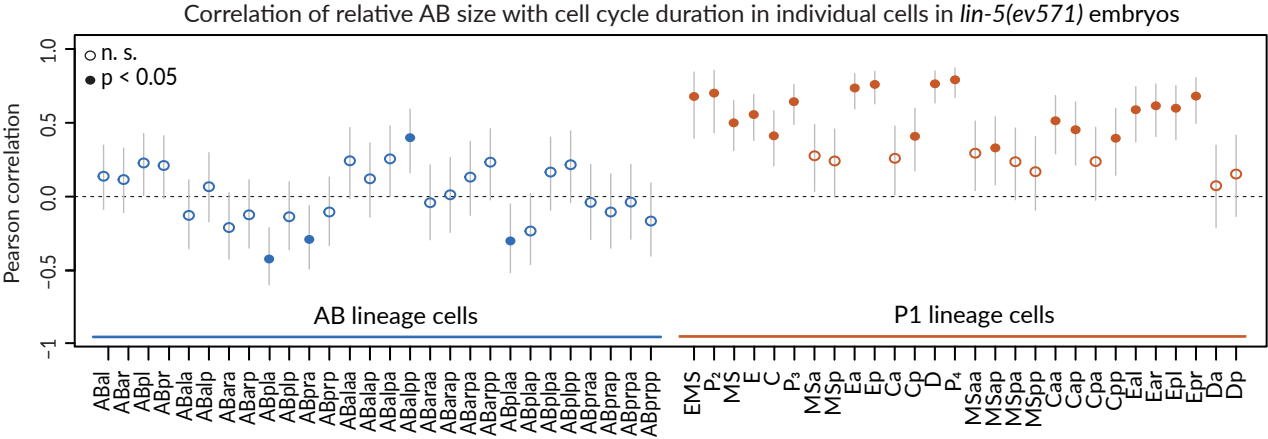


Figure 4

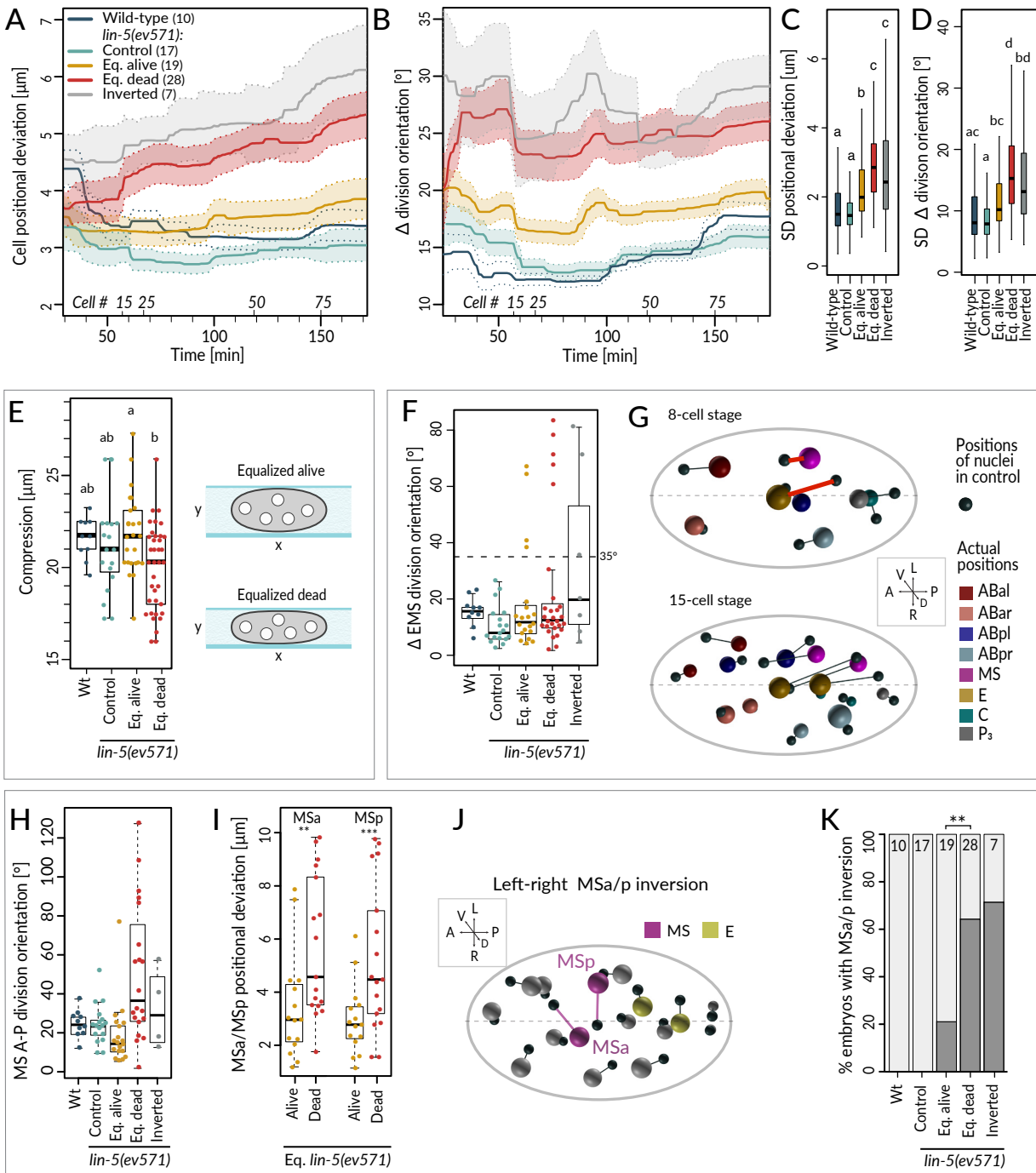


Figure 4 - supplement 1

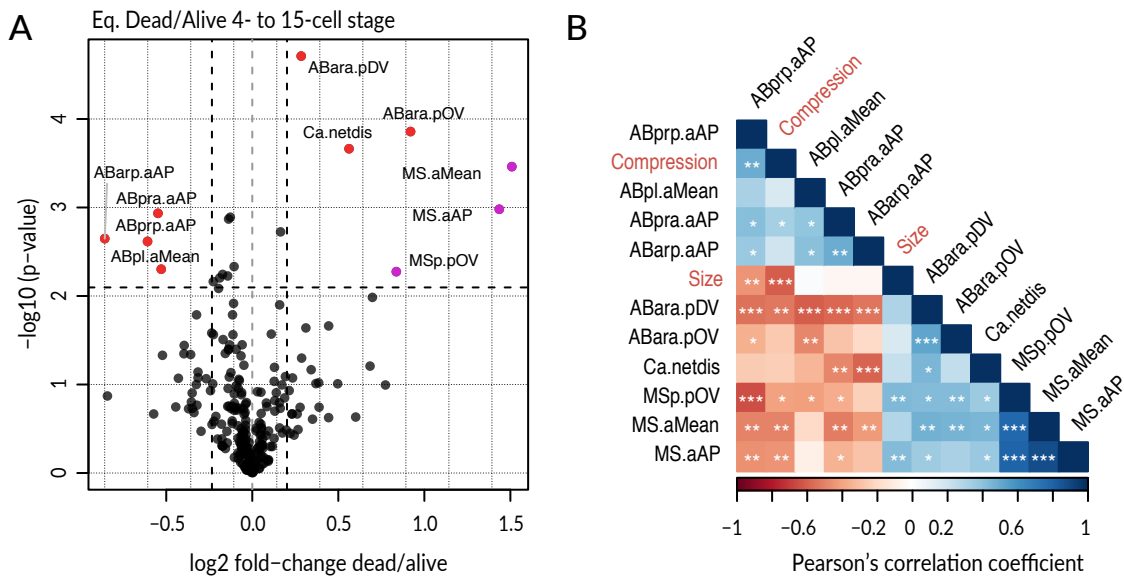


Figure 5

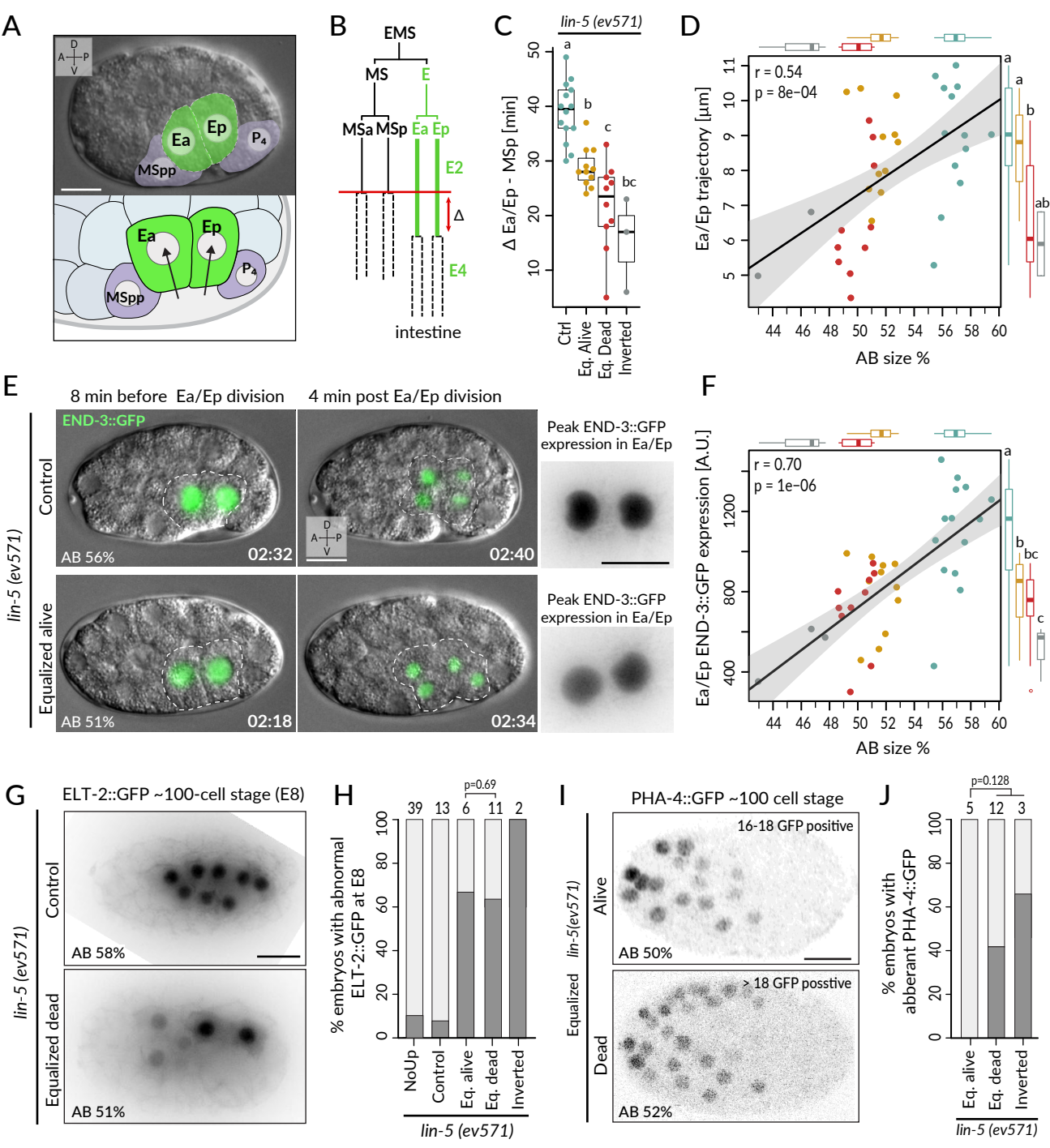


Figure 5 - supplement

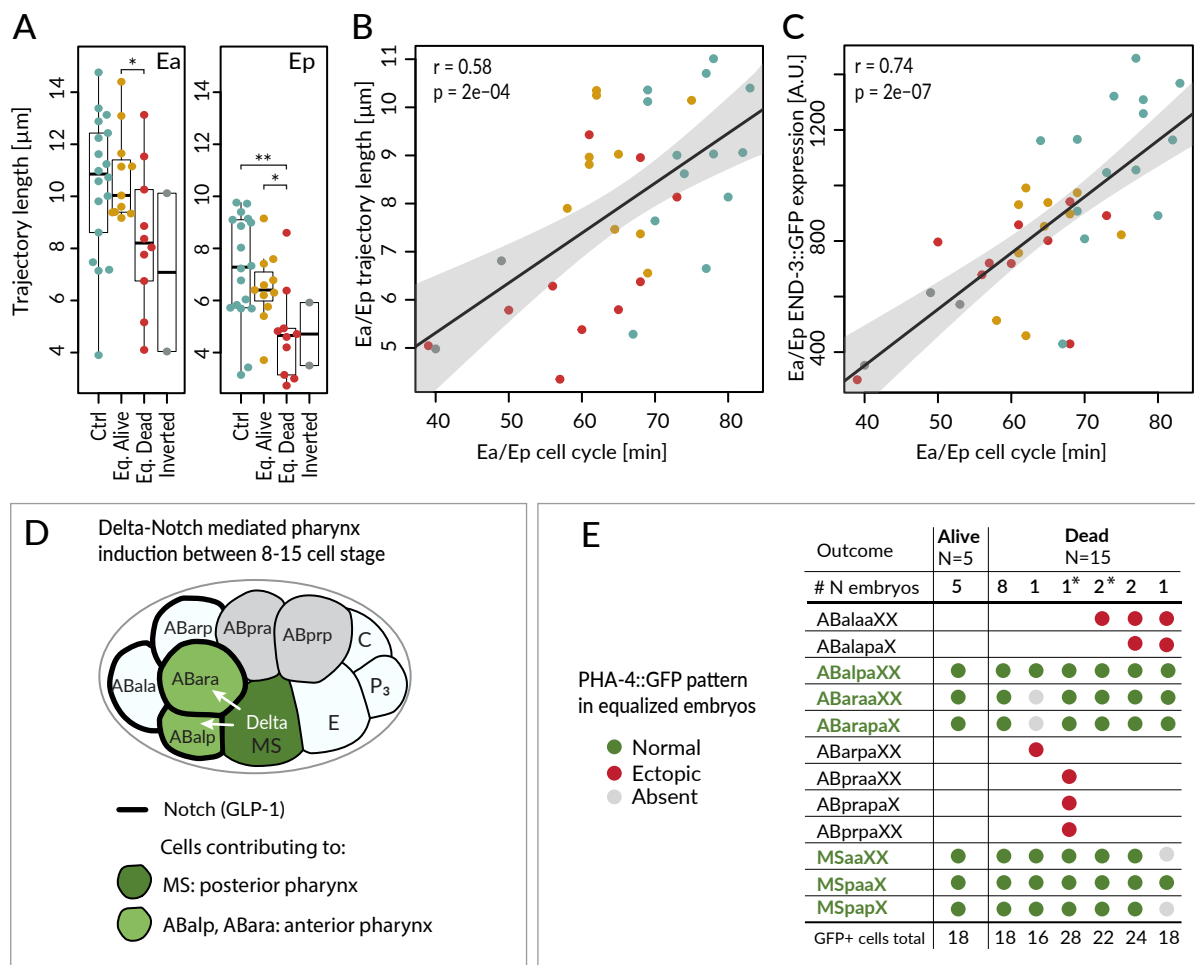


Figure 6

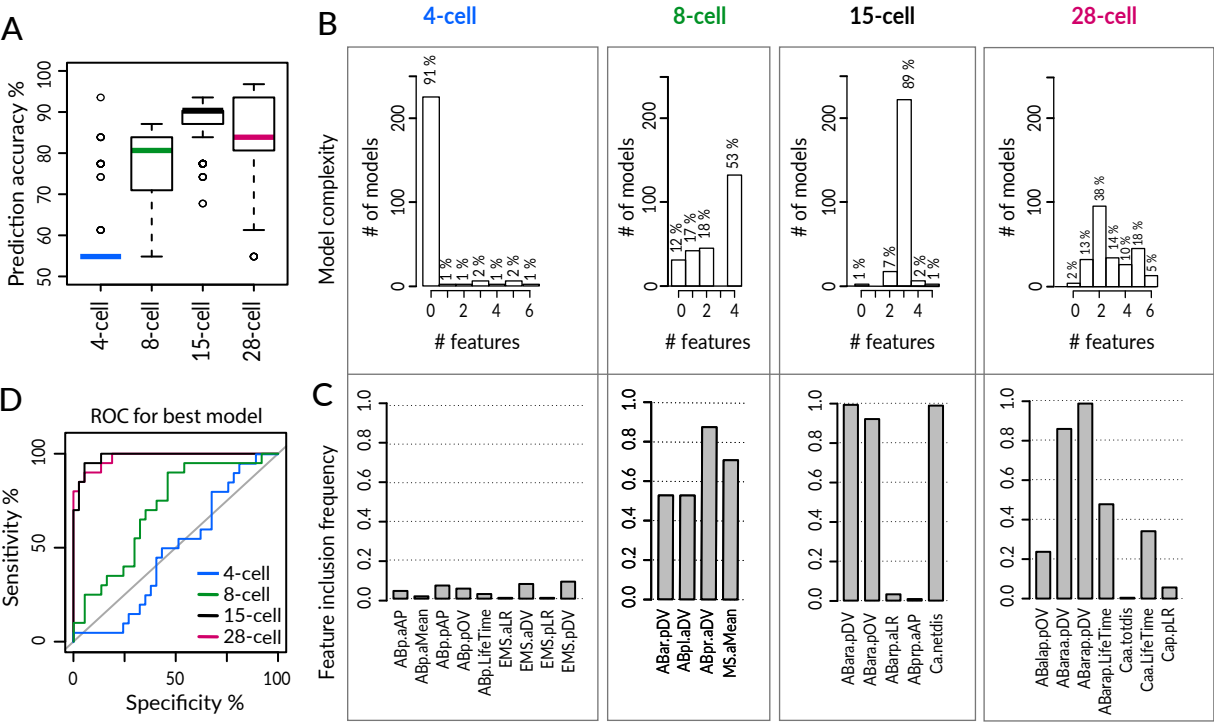


Figure 6 - supplement 1

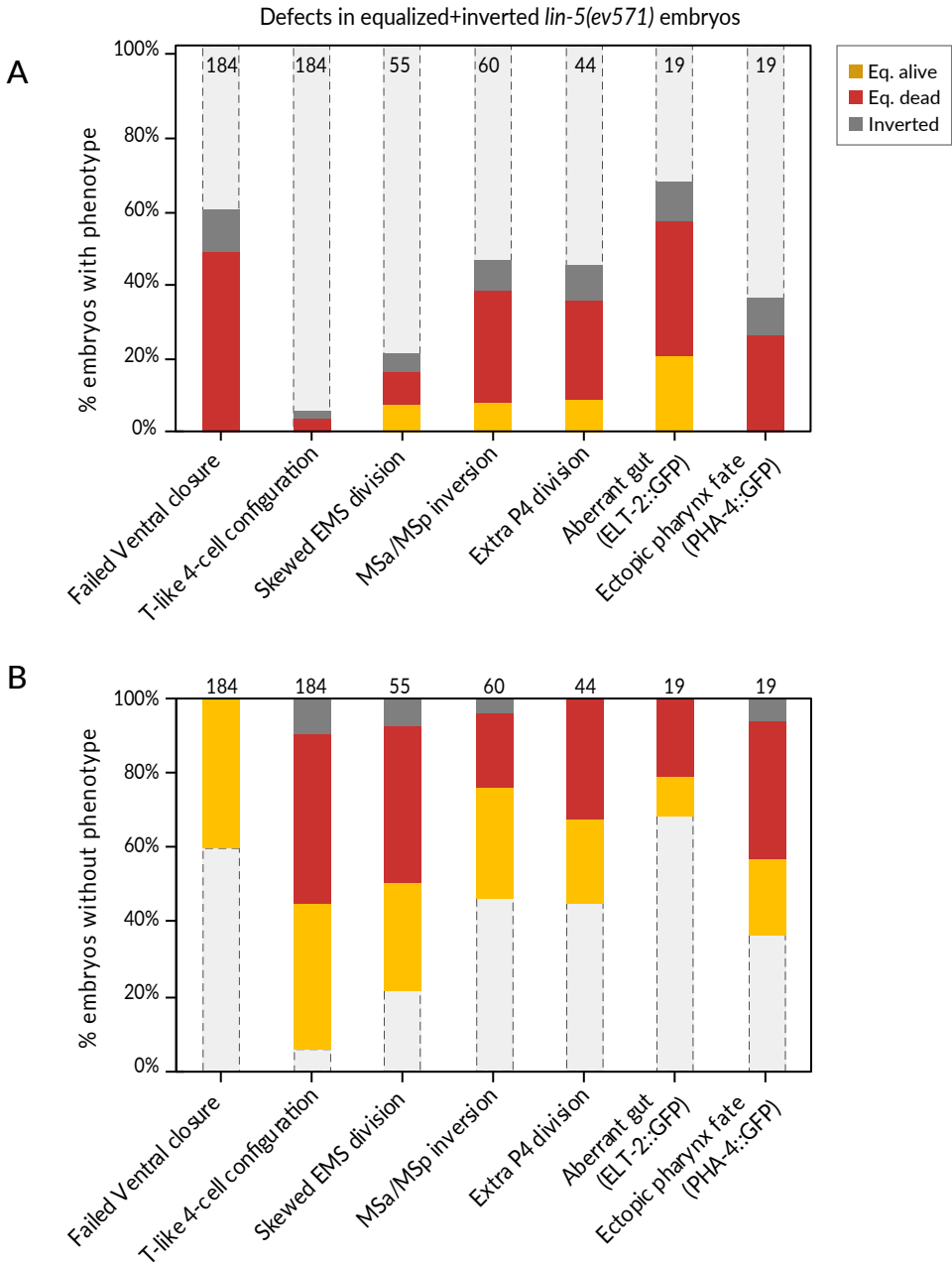


Figure 6 - supplement 2

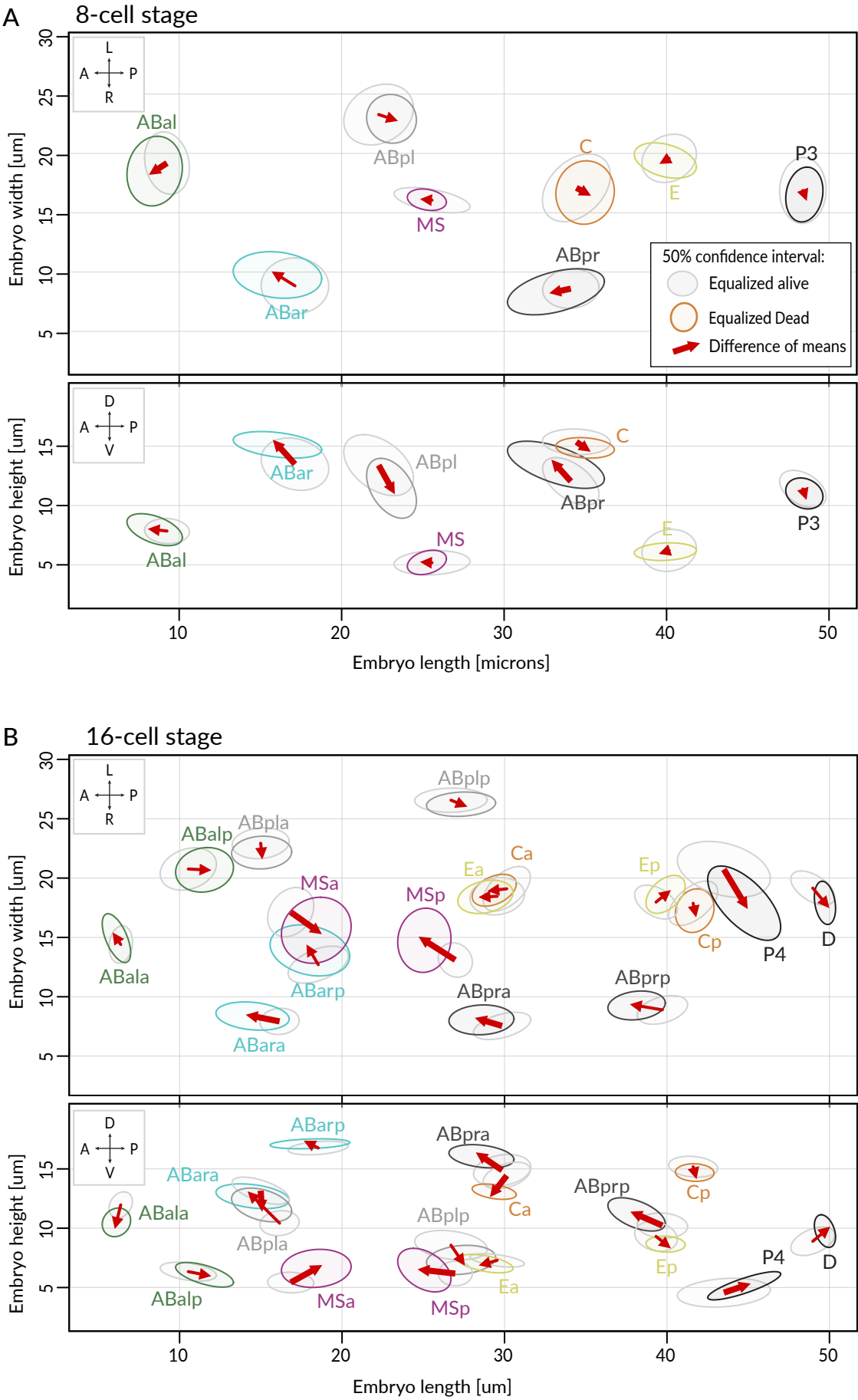


Figure 6 - supplement 3

